



1 **Evolution of the Iberian Massif as deduced from its crustal thickness and**
2 **geometry of a mid-crustal (Conrad) discontinuity**

3 Puy Ayarza¹, José Ramón Martínez Catalán¹, Ana Martínez García², Juan Alcalde², Juvenal Andrés^{1,2},
4 José Fernando Simancas³, Immaculada Palomeras¹, David Martí^{2,4}, Irene DeFelipe², Chris Juhlin⁵,
5 Ramón Carbonell²

- 6 1. Geology Department, Salamanca University. Pza de la Merced, s/n. Salamanca 37008. Spain
7 2. Geosciences Barcelona, CSIC. Lluís Solé i Sabaris, s/n. Barcelona 08028. Spain
8 3. Geodynamics Department, Granada University. Av/ de la Fuente Nueva, s/n. Granada 18071. Spain
9 4. Lithica SCCL. Avinguda Farners 16, Santa Coloma de Farners, Girona 17430. Spain
10 5. Department of Earth Sciences, Uppsala University. Villavägen 16, Uppsala, 75236. Sweden

11

12 Corresponding author: Puy Ayarza (puy@usal.es)

13 **Abstract**

14 Normal incidence seismic data provide the best images of the crust and lithosphere. When
15 properly designed and continuous, these sections greatly contribute to understanding the
16 geometry of orogens and, together with surface geology, to unravel their evolution. In this
17 paper we present an almost complete transect of the Iberian Massif, the westernmost
18 exposure of the European Variscides. Despite the heterogeneity of the dataset, acquired
19 during the last 30 years, the images resulting from reprocessing with a homogeneous workflow
20 allow us to clearly define the crustal thickness and its internal architecture. The Iberian Massif
21 crust, formed by the amalgamation of continental pieces belonging to Gondwana and
22 Laurussia (Avalonian margin) is well structured in upper and lower crust. A conspicuous mid-
23 crustal discontinuity is clearly defined by the top of the reflective lower crust and by the
24 asymptotic geometry of reflections that merge into it, suggesting that it has often acted as a
25 detachment. The geometry and position of this discontinuity can give us insights on the
26 evolution of the orogen, i.e. of the effects and extent of the late Variscan gravitational
27 collapse. Also, its position and the limited thickness of the lower crust in central and NW Iberia
28 constraints the response of the Iberian microplate to Alpine shortening. This discontinuity is
29 here observed as an orogeny-scale feature with characteristics compatible with those of the
30 worldwide, Conrad discontinuity.

31 **Keywords:** Iberian Massif, vertical incidence seismic data, mid-crustal detachment, Conrad
32 discontinuity, geodynamic evolution

33 **1. Introduction**

34 In the last 35 years, controlled source seismic data have greatly contributed to the
35 understanding of the European Variscides. National research programs like DEKORP (Bortfeld,
36 1985; DEKORP Research Group, 1987; Franke et al., 1990; Oncken, 1998), BIRPS and ECORS
37 (BIRPS and ECORS, 1986) have sampled this orogen providing a detailed picture of its
38 lithospheric architecture. In the Iberian Massif, normal incidence (NI) seismic reflection profiles
39 often acquired with coincident wide angle (WA) reflection/refraction seismic data have
40 allowed scientists to depict its crustal structure, infer its P and S waves velocity distribution,
41 place constraints on its geodynamic evolution, visualize the accommodation pattern of



42 shortening at different crustal levels and, sometimes, deduce the effect of Alpine reactivation
43 on this Paleozoic orogen.

44 In this regard, seismic datasets acquired in the Iberian Massif (De Felipe et al., 2020) from the
45 programs ESCIN (Ayarza et al., 1998, 2004; Pérez-Estaún et al., 1991; Pulgar et al., 1996),
46 IBERSEIS (Flecha et al., 2009; Palomeras et al., 2009; Simancas et al., 2003), ALCUDIA (e.g.,
47 Ehsan et al., 2014, 2015; Martínez Poyatos et al., 2012) and CIMDEF (Andrés et al., 2019) have
48 helped to identify several outstanding features such as, i) clear differences in the intensity and
49 geometry of reflectivity at upper and lower crustal levels, ii) contrasting deformation patterns,
50 and iii) a very reflective and sometimes thick lower crust, even in areas where the upper crust
51 is weakly deformed. In order to explain these features, decoupling of the upper and lower
52 crust has been invoked along large parts of the sampled area (Simancas et al., 2013). The
53 existence of a mid-crustal detachment has been addressed as the reason why different
54 shortening mechanisms exist at different crustal levels. However, coupled crustal deformation
55 has been inferred for NW Iberia, where large crustal thickening took place. Also, no inference
56 has been made on how this detachment acted during later Alpine deformation.

57 In this paper, we present a more complete seismic section of the Iberian Massif. We benefit
58 from the existence of new datasets (CIMDEF and ALCUDIA WA) that fill the gaps of areas
59 previously unexplored, like Central Iberia, altogether providing an almost complete transect.
60 Later on, we revisit the extension and implications of a mid-crustal discontinuity that, in our
61 view, exists below the entire Iberian Massif, certainly playing a critical role in the decoupling
62 between upper and lower crustal deformation. Finally, we infer the geometry and nature of
63 this feature and relate it with the long-debated (e.g., Finlayson et al., 1984; Litak and Brown,
64 1989; Wever, 1989; Xiaobo and Tae Kyung, 2010) Conrad discontinuity (Conrad, 1925).

65 **2. Geological setting**

66 The Iberian Massif represents the westernmost outcrop of the European Variscides, exposing
67 an almost complete section of this Paleozoic Orogen. It is divided into six zones (Fig. 1; Arenas
68 et al., 1988; Farias et al., 1987; Julivert et al., 1972) that from N to S and E to W are: Cantabrian
69 (CZ), West Asturian-Leonese (WALZ), Galicia-Trás-os-Montes (GTMZ), Central Iberian (CIZ),
70 Ossa-Morena (OMZ) and South Portuguese (SPZ). The CZ and the SPZ represent the external
71 zones whereas the rest represent the hinterland. The CZ, WALZ and CIZ belong to the northern
72 margin of Paleozoic Gondwana. The GTMZ represents the remnants of a large nappe stack
73 formed by pieces of the outermost margin of the Gondwana margin, i.e., a pulled-apart peri-
74 Gondwanan terrane and oceanic units derived from the oceanic realm separating them. They
75 were emplaced above the autochthonous CIZ in NW Iberia and are preserved as a large klippen
76 at the core of late Variscan synforms (Martínez Catalán et al., 1997, 2007; Ries and Shackleton,
77 1971). Its rootless suture (ophiolitic units) is thought to represent a branch of the Rheic
78 oceanic realm (Martínez Catalán et al., 1997). The OMZ has been interpreted as a continental
79 fragment that rifted and probably drifted away from Gondwana (Matte, 2001; Robardet,
80 2002), docking back later to the CIZ giving rise to a suture and thus representing another peri-
81 Gondwanan terrane (Azor et al., 1994; Gómez-Pugnaire et al., 2003; Simancas et al., 2001).
82 Finally, the SPZ is thought to be separated from the OMZ by the Rheic Ocean suture (Simancas
83 et al., 2003) which was later overprinted by early Carboniferous extension accompanied by



84 mafic intrusions (Azor et al., 2008) and by transpression (Pérez-Cáceres et al., 2015). In this
85 context, the basement of the SPZ represents a fragment of Avalonia (Braid et al., 2011, 2012;
86 Pereira et al., 2014; Rodrigues et al., 2015), and its correlation with the Rheno-Hercynian Zone
87 in Germany (Franke, 2000; Franke et al., 1990) further supports this affinity.

88 From a tectonic point of view, the Iberian Massif shows evidences of pre-Variscan activity. The
89 Cadomian Neoproterozoic event is characterized by continental arc magmatism, deformation
90 and metamorphism (Bandrés et al., 2004; Dallmeyer and Quesada, 1992; Ochsner, 1993). It
91 developed above a previous non-outcropping continental crust, and formed the basement
92 above which the Ediacaran and Paleozoic sedimentation took place, favored by Ediacaran-
93 Cambrian and Cambro-Ordovician rifting which developed a wide continental platform
94 (Linnemann et al., 2008; Sánchez-García et al., 2008, 2010). However, most of the tectonic
95 features observed in the surface are the result of the Devonian and Carboniferous collision
96 between Gondwana, some peri-Gondwanan terranes and the Avalonian border of Laurentia,
97 which resulted in the Variscan Orogen (Matte, 2001). The deformation associated to the latter
98 was diachronous along the Iberian Massif. Next, we describe it, from N to S (in present
99 coordinates), together with the most important stratigraphic features.

100 The CZ (Fig. 1) is an external zone located at the core of the Ibero-Armorican Arc (IAA; Dias and
101 Ribeiro, 1995; Lotze, 1929; Matte and Ribeiro, 1975; Stille, 1924). It is a thin-skinned thrust and
102 fold belt with a transport direction towards the foreland in the E, and overprinted by oroclinal
103 folding giving rise to the IAA (Alonso et al., 2009; Pérez-Estaún et al., 1988). Stratigraphically,
104 it is characterized by a Precambrian sequence, cropping out at its western part and overlain by a
105 Paleozoic stratigraphic succession that ranges from the Cambrian to a well-developed
106 Carboniferous: pre-orogenic up to early Carboniferous, and syn-orogenic in the Upper
107 Carboniferous (Sánchez de Posada et al., 1990; Truyols et al., 1990). Scarce tholeiitic and
108 alkaline magmatism is related to Cambro-Ordovician rifting (Corretgé and Suárez, 1990), and
109 no regional metamorphism accompanied deformation, indicating shallow crustal conditions. In
110 this area, deformation began at ~325-320 Ma, in the Late Mississippian (Dallmeyer et al.,
111 1997), and the emplacement of nappes that characterize the deformation and the formation
112 of folds within each sequence took place between the Westphalian B and the Stephanian (313-
113 300 Ma), in the Upper Carboniferous (Pérez-Estaún et al., 1988). An extensional episode
114 related to the end of the orogeny led to the formation of Permian Basins (Martínez García,
115 1981). Later on, extension related to the opening of the Bay of Biscay triggered the
116 development of deep Cretaceous basins (Quintana et al., 2015; Rat, 1988). Alpine tectonics
117 uplifted the Pyrenean-Cantabrian range from the end of the Late Cretaceous to the Miocene
118 (De Felipe et al., 2019; Teixell et al., 2018 and references therein) reactivating Variscan thrusts
119 and Mesozoic normal faults (Gallastegui et al., 2016).

120 The WALZ lies to the W of the CZ (Fig. 1). Stratigraphically it consists of a Neoproterozoic
121 terrigenous sequence uncomformably overlain by a Paleozoic platform succession that ranges
122 from the Cambrian to the Lower Devonian (Martínez Catalán, 1985), much thicker than that of
123 the CZ. These sediments were actively deformed along three compressional (C1, C2, and C3)
124 and two extensional (E1 and E2) phases during the Variscan Orogeny (Martínez Catalán et al.,
125 2014). Large E vergent folds witness the C1 related compression (360-340 Ma). Those were
126 later affected by E vergence thrusts resulting from ongoing shortening (345-325 Ma). Crustal



127 thickening followed by thermal relaxation led to syn-orogenic extension during E1 (330-315
128 Ma). A last compressional episode (C3, 315-305 Ma) produced upright folds associated with
129 wrench shear zones while simultaneous extension (E2, 315-300 Ma) continued, characterizing
130 the latest stages of the orogeny in this area. Crustal melting triggered by compression and
131 thickening led to extension and to the intrusion of granitoids in the western part of the WALZ.
132 Thermal models show that the crust could have started to melt within 30 Ma after the start of
133 crustal thickening, which is then constrained by the ages of Variscan granitoids (Alcock et al.,
134 2009).

135 The CIZ is the largest of the Iberian Massif zones. Curvature of magnetic anomalies and that of
136 early (C1) Variscan folds depict the Central Iberian Arc (CIA; Martínez Catalán, 2011a, 2011b),
137 partly explaining the width of this internal zone. The stratigraphic sequence differs from N to S:
138 Ordovician felsic metavolcanic, subvolcanic and intrusives (Díez-Montes et al., 2010) represent
139 the most ancient lithologies cropping out in the N, defining the 'Ollo de Sapo' domain whereas
140 to the S, Upper-Proterozoic-Lower Cambrian metasediments outcrop (Díez Balda, 1986; Díez
141 Balda et al., 1995), defining the 'Schist-Greywacke Complex' domain. The pre-orogenic
142 sedimentary sequence continues to the Devonian, followed by a syn-orogenic Carboniferous
143 sequence (Martínez Catalán et al., 2004; Robardet, 2002). This area represents a relatively
144 stable Gondwana margin characterized by the Early Ordovician extension that opened the
145 Rheic Ocean and allowed intrusion of essentially felsic magmas (Díez Montes et al., 2010). The
146 deformation phases described for the WALZ affected most of the CIZ although C1, C2 and E1
147 are somewhat older, according to the propagation of deformation from the hinterland. Slight
148 differences in the importance of phases can also be found to the center and S (Martínez
149 Catalán et al., 2019), allowing the CIZ to be divided in two zones. In the NW, intense
150 recumbent C1 folds and important C2 thrusts exist, related to the emplacement of the GTMZ.
151 Outcropping rocks show epi- to catazonal metamorphism and ductile detachments. Gneiss
152 domes of both E1 and E2 extensional phases exist, evidencing significant crustal thinning, and
153 Variscan granitoids are abundant. To the S, C1 folds are upright, C2 deformation is limited to
154 the southernmost part, and upright C3 folds are the most important structures (Martínez
155 Catalán et al., 2012; Martínez Poyatos, 2002). Metamorphism is generally weak and the
156 amount of granitoids decreases, except in the Iberian Central System (ICS). Here extension
157 postdates C3 upright folding and thus, it is considered E2.

158 Alpine tectonics in the CIZ reactivated previous Variscan fractures and triggered the
159 development of the Iberian Central System (ICS) mountain belt (de Vicente et al., 1996),
160 allowing the products of syn- and post-E2 crustal melting to outcrop in large areas.

161 The GTMZ is represented by five klippen that are the remnants of the emplacement of a thick
162 nappe stack on top of the CIZ. This includes, from bottom to top, a relatively distal part of the
163 northern Gondwana margin (Parautochthon), the outermost edge of that margin (Lower
164 Allochthon), a few oceanic units of Cambro-Ordovician and Lower Devonian age (Middle
165 Allochthon) and a peri-Gondwanan terrane with magmatic evidences of Cambro-Ordovician
166 rifting and a continental arc setting (Upper Allochthon). Several units show high-P
167 metamorphism reflecting subduction of the ocean represented by the Middle Allochthon and
168 involving also the Upper and Lower ones (Arenas et al., 2007; Gómez Barreiro et al., 2007;
169 Martínez Catalán et al., 2007; Sánchez Martínez et al., 2007). Ongoing subduction during most



170 of the Devonian (400-365 Ma) built an accretionary wedge that was subsequently emplaced on
171 top of the CIZ during the early Carboniferous (C2 event, c. 360-340 Ma).

172 The boundary between the CIZ and the OMZ (the Badajoz Córdoba Shear Zone) has been
173 largely interpreted as a suture (Gómez-Pugnaire et al., 2003; Simancas et al., 2001), although
174 no true oceanic units have been identified. It includes amphibolites of oceanic affinity from the
175 early Paleozoic, as well as eclogite relics. In SW Iberia, outcropping lithologies range from the
176 Upper Precambrian to the Upper Carboniferous, with an angular unconformity at the Lower
177 Carboniferous. In the OMZ, the Serie Negra is a thick Neoproterozoic sequence that includes
178 graphitic quartzites and schists and underwent Cadomian arc-related magmatism and regional
179 metamorphism (Dallmeyer and Quesada, 1992; Ochsner, 1993; Quesada and Dallmeyer, 1994).
180 The pre-orogenic Paleozoic sequence is rather complete and was deposited at the peri-
181 Gondwanan platform, as for the CIZ, although differences in the faunal content and in the
182 Paleozoic facies, generally more pelitic in the OMZ, point to a more distal position (Robardet,
183 2002; Robardet and Gutiérrez Marco, 1990). Ediacaran-Cambrian and Cambro-Ordovician
184 magmatism reflects two rifting events. The latter is the most important one, it includes alkaline
185 magmatism and is related with the opening of the Rheic Ocean (García Casquero et al., 1985;
186 Ochsner, 1993; Sánchez-García et al., 2008, 2010). The first deformation event, of Devonian
187 age, formed overturned and recumbent folds and thrust faults with SW vergence (Expósito et
188 al., 2002, 2003). Syn-orogenic, early Carboniferous basins developed in an extensional context
189 and are related to calc-alkaline volcanism and magmatism (Casquet et al., 2001). These
190 deposits unconformably overlay the early folds and thrusts. Later, deformation continued with
191 middle and upper Carboniferous sinistral transpression and associated upright NW-SE folds.

192 A salient seismic reflector, the Iberseis Reflective Body (IRB, Carbonell et al., 2004; Simancas et
193 al., 2003) seems to be the result of a mantle-derived intrusion located along a mid-crustal
194 detachment around 350-340 Ma. It was emplaced in the context of early Carboniferous
195 extension in the SW of the Iberian Massif, while the hinterland to the NW was undergoing the
196 first stages of compression (C1). Magmatic activity in the SW triggered a high-T/low-P
197 metamorphism that, otherwise, has a low grade elsewhere in the OMZ (Díaz Azpiroz et al.,
198 2006; Pereira et al., 2009).

199 The boundary between the OMZ and the SPZ has been long understood as a suture on the
200 basis of geometric assumptions (e.g., Carvalho, 1972). Later evidences have reinforced this
201 point of view suggesting that the above mentioned boundary represents the remnants of the
202 Rheic Ocean, although Carboniferous transtension and transpression have largely obliterated it
203 (Pérez-Cáceres et al., 2015 and references therein). The SPZ is a Variscan foredeep basin
204 strongly deformed by thin-skinned thrust tectonics, and is usually correlated with the
205 Rhenohercynian Zone of Kossmat (1927) in the Bohemian Massif. It features wide outcrops of
206 low or very low grade Devonian phyllites, quartzites and sandstones overlain by a lower
207 Carboniferous (Early Mississippian) volcano sedimentary sequence topped by middle and
208 upper Carboniferous flysch (Oliveira, 1990). From a tectonic point of view, it is characterized by
209 Carboniferous S vergent thrusts and folds, the latter featuring axial traces oblique to the
210 northern boundary of the zone, evidencing transpression (Simancas et al., 2003 and references
211 therein). Deformation propagated towards the S along the lower and upper Carboniferous
212 (Oliveira, 1990).



213 Although the start of the Variscan collision seems to have been frontal or maybe right-lateral
214 in most of Europe (Shelley and Bossière, 2000), surface geology and interpretation of seismic
215 data evidences the existence of relevant left lateral transpression and oblique-slip syn-
216 metamorphic shear zones in the OMZ, SPZ and their boundaries (Pérez-Cáceres et al., 2016;
217 Simancas et al., 2003 and references therein). In the OMZ, folds and thrusts witnessing
218 Devonian and early Carboniferous compression are oblique to the OMZ/SPZ boundary,
219 indicating a transpressional setting. These features are disrupted by later Mississippian
220 transtensional tectonics (Expósito et al., 2002) that gave way to the intrusion of the Beja-
221 Acebuches mafic and ultramafic rocks (Azor et al., 2008). Convergence resumed soon after,
222 leading to the emplacement of the Beja–Acebuches unit onto the OMZ (Pérez-Cáceres et al.,
223 2015). Inside the OMZ, Devonian and Carboniferous left lateral deformation accounts for ~400
224 km, higher than perpendicular shortening. Likewise, inside the SPZ, left-lateral displacement is
225 estimated to reach 90 km whereas the orthogonal one amounts ~60 km (Pérez-Cáceres et al.,
226 2016).

227 **3. Geophysical setting: Existing datasets, their reprocessing and a brief description**

228 **3.1. Seismic datasets sampling the Iberian Massif**

229 Since the early 90's, the Iberian Massif has been sampled by different controlled source
230 seismic experiments (De Felipe et al., 2020): the ESCIN (1991-1992), IBERSEIS (2000 and 2003),
231 and ALCUDIA (2007-2012) experiments acquired normal incidence (NI) and coincident wide-
232 angle (WA) data. The latest project, carried out with the target of understanding the structure
233 and effect of the Alpine reactivation across the central part of the Iberian Massif, is the
234 CIMDEF experiment (2017-2019). It acquired densely spaced controlled source WA reflection
235 and natural source (earthquakes and noise) seismic data. However, the acquisition of NI data
236 has not currently been planned along this transect, regardless of its potential quality and
237 relevance, due to the relatively high costs of this kind of experiments.

238 From N to S, and from E to W, the ESCIN project sampled the northern part of the Iberian
239 Massif (Fig. 1). Profile ESCIN-1 (1991) is an onshore E-W line crossing the CZ from its eastern,
240 most external part to its boundary with the WALZ to the W; Profile ESCIN-2 (1991) is an
241 onshore N-S profile crossing the most external and eastern part of the CZ and reaching the
242 northern end of the Duero Basin (DB) to the S, which represents the Cantabrian Mountains
243 foreland basin. The ESCIN-3 (1992) profiles sampled the WALZ and the CIZ along the northern
244 Iberia shelf. Although it consists of three parts (ESCIN-3.1, 3.2 and 3.3) only the easternmost
245 ones (3.2 and 3.3.) are relevant for the study of the Variscan crust and thus, included here.
246 ESCIN-3.3 crossed the entire WALZ to its western boundary with the CIZ, which in this area was
247 surveyed by the ESCIN-3.2. Geographically, the latter also sampled the allocthonous GTMZ.
248 But as this is an offshore profile, it shows no evidences of the presence of the GTMZ, and most
249 of the imaged crust corresponds to that of its relative autochthon, the CIZ.

250 A significant geographical and methodological gap exists between the ESCIN profiles to the N
251 and the location of the CIMDEF experiment (Fig. 1). The latter crosses central Iberia from the N
252 part of the CIZ, then samples the DB down to ICS, and goes on S across the Tajo Basin (TB) till it
253 reaches again the CIZ metasediments to the S of the ICS.



254 In the southern part of the Iberian Massif, the onshore ALCUDIA seismic line (NI and WA),
255 striking NE-SW, was acquired across the CIZ, going from the S of the ICS to the boundary with
256 the OMZ. Finally, the NE-SW IBERSEIS dataset (NI and WA) is also an onshore profile that
257 partially overlaps the same structures as the SW end of the ALCUDIA line although with some
258 50 km of offset to the W. This seismic line samples the southern part of the CIZ, the OMZ and
259 the SPZ.

260 Altogether these seismic profiles account for a ~1500 km long seismic transect geared to
261 understand the crustal and, in places, lithospheric structure of the Iberian Massif and to
262 constrain its evolution.

263 3.2. Processing of datasets

264 The data used in this work have been acquired at different times, have different characteristics
265 (onshore and offshore) and accordingly exhibit very heterogeneous quality. Table 1 shows the
266 acquisition parameters of all these datasets. The most outstanding differences are: i) the
267 quality and characteristics of the offshore (ESCIN-3) vs the onshore data, ii) the difference
268 between the low fold (30) ESCIN-1, ESCIN-2 and ESCIN-3 data acquired with an explosive
269 source and airguns respectively and the high fold (>60) IBERSEIS and ALCUDIA datasets, which
270 used Vibroseis trucks as source of energy, and iii) the fact that the CIMDEF dataset lacks NI
271 data and only provides lower resolution noise and earthquake data, since WA profiles are, as
272 yet, un-interpreted. Thus, reprocessing the NI data was mandatory, at least at stack and post-
273 stack level. Figure 2 shows the processing flow followed to homogenize the display of datasets
274 while preserving the true amplitude (Martínez García, 2019). The software package used for
275 reprocessing was GLOBE Claritas (www.globeclaritas.com/) and the most important steps were
276 related with frequency filtering, amplitude weighting and equalization, Kirchhoff time
277 migration and coherency filtering (Fig. 2). In addition, up to 20 multi-trace attribute analysis
278 were tested with the goal to enhance structural and lithological impedance contrasts that
279 allowed to improve the interpretation (Chopra and Alexeev, 2005; Taner and Sheriff, 1977).
280 Although this methodology has been mostly used in sedimentary reservoirs, we have seen that
281 the application of these techniques can enhance the continuity of reflections and help to
282 identify different types of crust, thus easing the interpretation. Some of the results of this
283 attribute analysis are included in the interpretations.

284 3.3. Description of the seismic sections

285 The NI datasets included in this paper have already been presented, so the reader will be
286 referred to previous publications for detailed descriptions of pre-stack processing and
287 interpretations. Here we will just focus on those features that are essential to our
288 interpretation.

289 Reprocessed migrated sections and their interpretations are presented in figure 3 (ESCIN-1),
290 figure 4 (ESCIN-2), figure 5 (ESCIN-3.3), figure 6 (ESCIN-3.2) figure 7 (ALCUDIA) and figure 8
291 (IBERSEIS). The description of sections will be done from N to S and from E to W. The CIMDEF
292 dataset will be described in the discussion (Figs. 9 and 10) as it is key to understanding the
293 geometry of the mid-crustal discontinuity, its late Variscan reworking and its Alpine
294 reactivation.



295 **3.3.1. Cantabrian Zone (ESCIN-1 section)**

296 The ESCIN-1 section is a ~130 km long, E-W profile crossing the CZ from its most external part
297 to the Narcea Antiform to the W, in the boundary with the hinterland (WALZ, Figs. 1 and 3). It
298 consists of two slightly overlapping parts, 1.1 and 1.2, separated a few kilometers in the N-S
299 direction. The complete ESCIN-1 section migrated at $v=5600$ m/s (Fig. 2) and its interpretation
300 are presented in figure 3.

301 This section was first described and interpreted over an unmigrated image by Pérez-Estaún et
302 al. (1994). Later works revisited the interpretation, adding travel-time modeling to help on the
303 understanding of the unmigrated data (Gallastegui et al., 1997). The reader is referred to these
304 papers for further details than those provided here.

305 In the upper crust, the western part shows W-dipping reflections that represent the Variscan
306 imbrication of the basement under the Paleozoic sequence (a in Fig. 3), indicating the
307 proximity of the hinterland (WALZ). In fact, a Neoproterozoic, non-metamorphic sequence
308 outcrops in this area, which is probably underlain by an older crystalline basement. One
309 prominent reflection (a') crosscuts subhorizontal ones, defining a pattern that might indicate
310 its slightly out of the plane provenance. To the E, the thin skinned tectonics characteristic of
311 this external zone can be interpreted from shallow subhorizontal to W dipping reflections (b).
312 The main one among these, running at around 5 s (TWT), is interpreted as the sole thrust of
313 the thin-skinned orogenic wedge (c). To the W, it gets involved in the crustal ramp observed at
314 the Narcea Antiform, suggesting that it ends down rooting into the upper part of the lower
315 crust (d). A low reflectivity wedge of undifferentiated basement (e) located between 4-5 and
316 8.5 s (TWT) exists underneath the easternmost reflections. This may image some pre-Paleozoic
317 basement that is interpreted as upper crust, since the pattern of reflections changes below,
318 suggesting that a significant boundary occurs underneath.

319 The lower crust shows little reflectivity but seems to be present in the interval between 8.5-14
320 s (TWT) in the E and between 8.5 and 12 s (TWT) in the W. It features subhorizontal (f) and W
321 dipping reflectivity to the E, the latter (f') crosscutting the former reflections. These might
322 represent the imprint of Alpine tectonics over a previously deformed/reflective lower crust. To
323 the W, reflectivity seems to be subhorizontal or dipping to the E (g). Some of the dipping
324 reflectivity observed at the edges of section ESCIN-1 might be related to the migration effects
325 over a little reflective section and caution should be taken when interpreting it.

326 The Moho along this section is located at nearly 14.5 s TWT (~45 km) in the eastern part, and
327 shallower (12 s TWT, ~36 km) to the W. The crustal thickening observed to the E (h) is probably
328 related with an out of section image of the crustal Alpine root, better observed in profile
329 ESCIN-2, which is described next.

330 **3.3.2. Cantabrian Zone and Duero Basin (ESCIN-2 section)**

331 The ESCIN-2 seismic line is a 65 km long, N-S section that samples the transition between the
332 CZ and the DB (Fig. 1). Even though this profile was geared to study the Alpine structures, it
333 shows how the Variscan features have been inherited and reactivated during the Cenozoic
334 compression between the Iberian Peninsula and the European plate. The section was first



335 presented by Pulgar et al. (1996). Later on, some authors have used this image to constraint
336 the Alpine structure in the North Iberian Margin (e.g., Fernández-Viejo et al., 2000; Gallastegui
337 et al., 2016). However, only Teixell et al. (2018) used a migrated version (4000 m/s) of this
338 section. Here we present the results of a Kirchhoff time migration at 5600 m/s (Fig. 4).

339 This seismic line shows, in places, a conspicuous reflectivity that allows a straightforward
340 interpretation. To the S end, the upper crust is characterized by high amplitude horizontal
341 reflectivity representing the DB sedimentary sequence. It occupies the interval from 0-3.5 s
342 TWT (a in Fig. 4) and appears to be offset by N dipping reflections (b). The latter have been
343 interpreted as S vergent Alpine thrusts affecting the CZ basement and partly the DB sediments.
344 The rest of the crust is less reflective although N dipping reflectivity (c), also interpreted as
345 imaging Alpine thrusts, crosscuts shallow subhorizontal weak reflections that represent the
346 Paleozoic sedimentary sequence of the CZ (d).

347 The lower crust presents higher amplitude reflectivity. In general, a thick band of horizontal
348 reflections located between 7.5 and 12 s (TWT) at the southern part of the profile, bends and
349 dips to the N in the northern part of the line (e) in response to Alpine compression. Although
350 the stacked section shows that this N dipping reflectivity reaches 14.5 s TWT (Pulgar et al.,
351 1996) the migrated sections (Teixell et al., 2018 and Fig. 4) indicate that these reflections move
352 southward and upward to less than 14 s (TWT), while losing amplitude and coherence. In fact,
353 the geometry of the bottom of the lowermost crust (Moho) is deduced on the basis of the
354 geometry of its uppermost part, the lower crust internal reflectivity, and the amplitude
355 contrasts observed in the attribute analysis (Fig. 4). Furthermore, its depth is solely established
356 on the basis of the position of the strongest subhorizontal reflections to the S.

357 Even though this profile shows the imprint of recent Alpine shortening, no reflections are
358 observed to crosscut the entire crust. In contrast, reflectivity suggests that deformation is
359 decoupled between the upper and lower crust. However, this section is not long and/or
360 reflective enough as to image where the Alpine thrusts (c) root. Possibly, they merge into the
361 roof of the underthrust CZ lower crust. In addition, the migration effects on the edges of the
362 section produce misleading reflectivity than hinders more detailed interpretations.

363 3.3.3. West Asturian-Leonese Zone (ESCIN-3.3 section)

364 The ESCIN-3.3 profile is part of a ~375 km long crooked offshore seismic line consisting in
365 ESCIN-3.1, 3.2 and 3.3. The latter is 137 km long, parallel to the coast and close to it across the
366 WALZ (Fig. 1). It was first presented by Martínez Catalán et al. (1995) and Ayarza et al. (1998,
367 2004). Later on, its image has been used to constrain the structure of the western North
368 Iberian Margin and that of the transition between the WALZ and the CIZ (Martínez Catalán et
369 al., 2012, 2014).

370 Reflectivity in the upper crust is characterized by the image of Mesozoic sedimentary basins (a
371 in Fig. 5) related to the extension that led to the opening of the Bay of Biscay. Underneath, W
372 dipping reflections are interpreted as the imprint of the first stages of Variscan compressional
373 deformation in the WALZ (C1 and C2), developing E-vergent thrust faults (b). These affect the
374 pre-Paleozoic basement and root in the upper part of a thick reflective band interpreted as the
375 lower crust (c) or in a sole thrust (d) that also reaches the lower crust.



376 The lower crust (c) is represented by a thick band of subhorizontal reflectivity (8-12 s TWT)
377 that thickens (6-12 s TWT) in the westernmost part of the WALZ (CDP 3000) underneath the
378 Lugo Dome, an extensional structure bounded to the E by the Viveiro normal fault (Fig. 5).
379 Then it thins towards the end of the line, when entering the CIZ, thus defining a Moho offset of
380 ~2 s TWT. The ESCIN-3.3 lower crust seems to feature an internal layer with mantle P-wave
381 velocities when modeled from coincident WA data. Accordingly it was interpreted as consisting
382 of the WALZ lower crust underthrust by the CZ lower crust (Ayarza et al., 1998). This model
383 would compensate the high shortening observed in the upper crust of the CZ, a thin-skinned
384 belt whose sole thrust roots at the contact with the WALZ. However, the ESCIN-3.3 WA data
385 need to be revisited as it is a fan profile difficult to model with old conventional 2D algorithms.
386 The internal reflectivity of the lower crust shows W dipping reflectors (e), similar to the ones
387 observed in the upper crust and probably imaging Variscan deformation in the lower crust,
388 either compressional or extensional. They crosscut subhorizontal reflectivity, thus postdating
389 it.

390 Even though migration over discontinuous reflections blurs the seismic section in the edges,
391 reflectivity never seems to cross-cut the crust and/or the Moho, indicating that deformation is
392 decoupled at upper and lower crustal level. Subcrustal E dipping reflections are interpreted as
393 the out-of-the-plane image of the Alpine southward subduction of the Bay of Biscay oceanic
394 crust (Ayarza et al., 1998, 2004), which is out of the scope of this paper.

395 The boundary between the WALZ and the CIZ is the Viveiro Fault, one of the most striking
396 surface expressions of Late Variscan extensional tectonics. To its W, gravitational collapse of a
397 thickened crust and associated crustal extension and melting have played a key role in the
398 orogenic evolution of the CIZ. However, to the E, crustal re-equilibration after C1 and C2
399 thickening was less important and igneous activity decreases. Even though this fault itself is
400 not identified in the seismic section (Fig. 4), the reflectivity in general varies on both sides of it,
401 featuring a thinner (9 s TWT vs 12 s TWT) and more transparent crust to the W. In fact the
402 geometry of some reflections (f) in the boundary between the WALZ and the CIZ, above the
403 thickest lower crust, and the subtractive way the sole thrust (d) merges with the lower crust
404 (d') seem to indicate the effect of extensional tectonics, sometimes reactivating compressional
405 structures (d-d'). Such a reactivation has been described for the base of the main thrust sheet
406 in the WALZ based on structural and metamorphic considerations (Alcock et al., 2009).
407 Conversely, further to the E of the section, reflectivity probably represents the geometry of
408 preserved compressional deformation.

409 **3.3.4. Northern Central Iberian Zone (ESCIN-3.2 section)**

410 The seismic line ESCIN-3.2 is a 97 km long profile, also parallel and close to the coast, and
411 sampling the relative autochthon to the GTMZ, i.e. the CIZ (Figs. 1 and 6). It was first described
412 by Álvarez-Marrón et al. (1996) and later by Ayarza et al. (2004).

413 This profile shows, in the upper part, a band of high subhorizontal reflectivity related to
414 Mesozoic basins, as in profile ESCIN-3.3 (a in Fig. 6). The rest of the upper crust is not very
415 reflective although a couple of W-dipping reflections (b) rooting in a thin band of strong
416 reflectivity are observed. These reflections, located in the E of the section from 4.5 s to 8 s
417 TWT, define a sort of duplex, extensional or compressional, but later extended, indicating in



418 any case boudinage and crustal thinning. To the W, the upper crust is very transparent and just
419 a few weak reflections can be observed.

420 The narrow reflective band at 8-9 s TWT represents the lower crust, and is the most striking
421 feature of this profile. This 1 s TWT thick feature contrasts with the neighboring ESCIN-3.3 and
422 even ESCIN-1 sections, which show a much thicker lower crust (4-5 s TWT). Reflectivity in this
423 band is subhorizontal (c), although somewhat undulated, while the band itself is slightly
424 inclined to the W. In the E, the Moho is located at around 9 s TWT (~27 km), the shallowest
425 identified so far in the Iberian Massif. Subcrustal dipping reflections (d) are again associated to
426 the 3D image of the southward subduction of the oceanic crust of the Bay of Biscay during the
427 Alpine convergence. They have been already modeled by Ayarza et al. (2004) and will not be
428 further discussed in this paper.

429 This profile samples the northern CIZ, where Variscan crustal thickening during C1 and C2, was
430 most important. Consequently, later gravitational collapse triggered extensional tectonics and
431 crustal melting, allowing the intrusion of granites and the development of extensional
432 detachments (with associated metamorphic offsets). The image of line ESCIN-3.2 shows a
433 transparent upper crust to the W suggesting that granites occupy most of it, which is
434 supported by onland geological mapping. Some thrust faults, as those imaged by W-dipping
435 reflections in profile ESCIN-3.3, probably root here and are represented by the W-dipping
436 reflections (b) at the base of the upper crust. However, these were later flattened and/or
437 reactivated as extensional detachments by crustal thinning. The narrowness of the highly
438 reflective lower crust here suggests that crustal thinning was largely accommodated at this
439 level, as the upper crust has basically the same thickness as in the ESCIN-3.3 line (up to 6-7 s
440 TWT). In addition, crustal melting might have also affected the top of the lower crust. But even
441 though large parts of the crust were melted, reflectivity exists deep in the upper crust,
442 suggesting that crustal melting was not pervasive and/or reflectivity is linked to syn- or late-
443 tectonic features.

444 **3.3.5. Southern Central Iberian Zone (ALCUDIA section)**

445 The ALCUDIA seismic profile was first presented by Martínez Poyatos et al. (2012) and
446 processed and further interpreted by Ehsan et al. (2014). It is a more than 220 km long, NE-SW
447 seismic profile sampling the CIZ to the S of the ICS down to the boundary with the OMZ (Fig. 1).

448 This profile presents a fairly transparent upper crust where scarce reflectivity to the S is related
449 to the boundary (suture) between the CIZ and the OMZ, namely, the Central Unit (CU; a in Fig.
450 7) and to the presence of vertical folds (b). Some very transparent zones (c) appear to be in
451 relation with the existence of granitic batholiths. To the N, the intrusion of these granites,
452 associated to the existence of normal faults (d), is one of the evidences of extensional
453 tectonics affecting the southern part of the CIZ. The rest of the upper crust shows weak and
454 discontinuous reflectivity that responds to the existence of vertical folding affecting lithologies
455 with little impedance contrast. In fact, deformation in the upper crust of this part of the CIZ is
456 weak, with absence of low-dipping structures typical of tangential tectonics.

457 The lower crust shows a very different image to that of the upper crust. It is a thick band, of up
458 to 6 s TWT (from 4 s to 10 s), of mostly subhorizontal high amplitude reflectivity (e) that at



459 some points appears to be cut across by N-dipping reflectors (f). S-dipping internal reflectivity
460 is also identified although more scarce (g). The lower crust thins in the northern end of the
461 profile, near the ICS, where intrusion of granites and other evidences of crustal re-equilibration
462 suggest that extension played a key role. Accordingly, we suggest that the mechanisms that
463 triggered this lower crustal thinning are related with melting and extension and not with
464 compression, as previously proposed (Ehsan et al., 2014; Martínez Poyatos et al., 2012), and
465 that the N dipping reflectivity observed above the lower crust in that area (h) is the expression
466 of extensional tectonics.

467 One of the most striking features of this profile is the crocodile-like structure affecting the
468 lower crust at around CMP 10000 (f). This structure, most likely related to Variscan shortening,
469 accommodates an important part of the deformation at lower crustal level and evidences that
470 sub-horizontal reflectivity of the lower crust is pre-Variscan, thus raising the question about its
471 precise age and origin. Despite the presence of this feature in the depth continuation of the
472 suture between the CIZ and the OMZ, reflectivity does not crosscut the whole crust, suggesting
473 the existence of a detachment in the top of the lower crust. This contrasts with the presence in
474 the upper crust (CU) of retro-eclogites with peak metamorphic conditions of 19 kbar and
475 ~550°C (López Sánchez-Vizcaíno et al., 2003). Finally, the Moho boundary is located at a fairly
476 constant depth (~10 s TWT, i.e. 30-33 km), although the lower crust seems to be preserved and
477 a local crustal imbrication into the mantle is observed underneath the crocodile-like structure.

478 3.3.6. Central Iberia, Ossa-Morena and South Portuguese Zones (IBERSEIS section)

479 The IBERSEIS seismic line was first presented by Simancas et al. (2003). A number of later
480 works added information and details to its interpretation (e.g., Carbonell et al., 2004;
481 Schmelzbach et al., 2007, 2008; Simancas et al., 2006). This section crosses the southernmost
482 CIZ, the whole OMZ, and most of the external SPZ (Fig. 1). It samples two major boundaries
483 interpreted as suture zones: that between the CIZ and the OMZ (CU, Azor et al., 1994) and the
484 one bounding the OMZ and the SPZ, which has been largely affected by young Carboniferous
485 events (Pérez-Cáceres et al., 2015). The IBERSEIS profile structurally overlaps the ALCUDIA
486 profile along ~30 km, but it is displaced some 50 km to the W. Its interpretation is shown in
487 figure 8.

488 This section is ~300 km long and features an outstanding reflectivity at upper and lower crustal
489 levels. In the upper crust, a wealth of N dipping reflections (a in Fig. 8) image a S verging thrust
490 and fold belt. In the SPZ, the most reflective events are probably related with normal faults
491 derived from the extension that led to the opening of the Rheic Ocean and were later
492 reactivated as thrusts during the Late Carboniferous compression. Some authors link the
493 highest reflective features to the middle Carboniferous volcano-sedimentary complex
494 (Schmelzbach et al., 2008), which might have used these fractures as a conduit, thus enhancing
495 reflectivity. In the OMZ, N dipping reflections probably image Variscan thrust faults as some
496 coincide with such mapped structures. Their lesser reflectivity might indicate the lack of
497 involvement in the thrusts of lithologies that increase the impedance contrast.

498 Upper crustal reflectivity in both, the ZOM and SPZ, does not cross to the lower crust, rooting
499 at a mid-crustal level that, in the SPZ is transparent and does not have any particular
500 expression itself. However, in the OMZ, a reflective layer exists at this depth (b): it has been



501 defined as the IBERSEIS reflective body (IRB, Simancas et al., 2003), a 140 km long, high
502 velocity conductive feature (Palomeras et al., 2009) that is supposed to represent an early
503 Carboniferous mantle-derived intrusion. Its origin has been related to mantle plume activity
504 that thinned the lithosphere and extracted mantle-derived melts from the ascending
505 asthenosphere (Carbonell et al., 2004). Its surface expression are intraorogenic transtensional
506 features (Rubio Pascual et al., 2013; Simancas et al., 2006). Alternatively, Pin et al. (2008) have
507 suggested, based on geochemical constraints, a tectonic scenario of slab break-off for this
508 feature. Internal reflectivity along the IRB is mostly subhorizontal, probably due to the effect of
509 the intrusion along a subhorizontal detachment, and evidences little imprint from Variscan
510 deformation. The body is slightly inclined to the S, at odds with the detachment being the sole
511 thrust of the OMZ upper crustal imbricates. Perhaps it was, but its inclination changed during
512 subsequent deformation, as later suggested.

513 The lower crust shows slightly different patterns in the CIZ and OMZ on one side and the SPZ
514 on the other. In the southernmost part of the CIZ and northern OMZ, N and S dipping
515 reflections define a wedge (c) that might be the western continuation of the crocodile-like
516 structure observed in the ALCUDIA seismic line in an equivalent structural position (f and g in
517 Fig. 7). In this section, the limited crustal imbrication into the mantle identified in the ALCUDIA
518 line is not observed, perhaps because it only occurs further to the N or E. This structure may be
519 the reason why the IRB is shallower at this point, indicating that the latter is older than the
520 crocodile compressional feature. The rest of the lower crust shows S dipping (d) and sub-
521 horizontal (e) reflectivity that does not exhibit clear crosscutting relationships, thus hindering
522 their interpretation. However, near the boundary with the SPZ, this reflectivity seems to be
523 affected by N dipping features (f) overprinting them. In the SPZ, the lower crust shows a more
524 homogeneous image, with subhorizontal reflectivity (g) that is often cut across by longer scale
525 S dipping features (h) that postdate them. The latter probably represent fractures that firstly
526 accommodated the extension linked to the opening of the Rheic Ocean and were then
527 reactivated as thrusts during the late Carboniferous compression and collision of the SPZ
528 basement with the OMZ. The most conspicuous of these reflections (h') cuts the IRB in its
529 southern part and seems to offset the lower crustal upper boundary between the SPZ and the
530 OMZ.

531 Even though the lower crust in the OMZ and SPZ shows dipping features, none of them cross
532 to the upper crust, thus rooting at a mid-crustal level as does the upper crustal reflectivity. This
533 implies again the existence of a discontinuity in the mid-crust.

534 Despite of crossing two suture zones and imaging part of a crocodile-like structure, the
535 IBERSEIS profile shows a fairly flat Moho located at ~ 10 s TWT, the same apparent depth as in
536 the ALCUDIA line (30-33 km). Its signature is very clear underneath the SPZ and a bit blurry
537 below the IRB.

538 4. Discussion

539 Simancas et al. (2013) already undertook an integrated interpretation of most of the seismic
540 sections presented here focusing on, i) the accommodation of orogenic shortening at crustal
541 scale, ii) the relationships between convergence, crustal thickening and collisional granitic
542 magmatism, and iii) the development of the Iberian Variscan oroclines. In this paper the same



543 sections are presented, but they have been reprocessed at stack level and time migrated using
544 a Kirchhoff algorithm. In addition, two extra sections that image the alleged mid-crustal
545 discontinuity after the Alpine reactivation are taken into account. The first one is the N-S
546 ESCIN-2 NI dataset (Fig. 4), in the CZ, where this discontinuity has remained untouched during
547 late Variscan evolution but was reactivated during the Alpine Orogeny. The second one results
548 from the CIMDEF experiment, carried out in the CIZ across the ICS, where the mid-crustal
549 discontinuity has probably been affected by crustal melting during the Late-Variscan extension
550 and by later Alpine reactivation. The latter sections somehow fill the gap existing in Simancas
551 et al. (2013).

552 Figures 3 to 8 represent an effort to show a homogeneous seismic image of the Iberian Massif
553 crust that eased its integrated interpretation. Next, we discuss the main observed features,
554 their implications and how they contribute to the understanding of the structure and evolution
555 of the Iberian Massif, adding constraints to the origin of the elevation of the central Iberian
556 Peninsula. Figure 9 presents a simplified sketch of the crustal layers observed in the Iberian
557 Massif. Figure 10 shows a compendium of the position of the mid-crustal discontinuity and the
558 Moho depth (in TWT) along the entire Iberian Massif as deduced from seismic NI data together
559 with a map of the entire Iberian Peninsula Moho depth (Palomeras et al., 2017) that includes
560 the position of the seismic profiles for comparison. We will refer to these figures along most of
561 the discussion.

562 A particular feature of the SW Iberian Massif is the great importance of out-of-section, mainly
563 left-lateral shear zones associated to its suture boundaries. They displaced central and
564 northern Iberia to the NW with respect to southern Iberia (Simancas et al., 2013). The seismic
565 sections do not provide constraints about this movement, as it is perpendicular to their layout.
566 Thus, interpretations in these areas must be taken with caution.

567 **4.1. The upper crust in the Iberian Massif: a depth image of outcropping geology**

568 Most of the seismic sections display a moderate to thick upper crust (4 to 8 s TWT, Fig. 9), with
569 very variable reflectivity. Reflections have been confidently related to outcropping Variscan
570 structures. As such, N dipping reflectivity in the SPZ and the OMZ is related to S vergent folds
571 and thrust faults mapped in the surface. W dipping reflections in the CZ are related to mapped
572 thin-skinned thrusts. The same type of reflectivity observed in the WALZ, reaching deeper
573 levels in the crust and rooting in the lower crust, has been addressed as evidence of thick-
574 skinned thrust tectonics, which in the hinterland affects the pre-Paleozoic basement.
575 Particularly interesting is the upper crustal SPZ seismic image in contrast with that of the CZ,
576 both representing external zones. While in the latter thrusts are observed to root in a shallow
577 sole detachment, in the former one reflections/thrusts root in the lower crust. This feature will
578 be discussed in the next section.

579 Only a few seismic profiles feature a transparent upper crust. Lack of reflectivity has been
580 related to low fold data (ESCIN-1 and ESCIN-2, Figs 3 and 4), and most importantly to the
581 existence of a re-equilibrated upper crust having recorded large amounts of partial melting, as
582 shown by voluminous outcropping granitoids (ESCIN-3.2 and N of ALCUDIA, Figs. 6 and 7). The
583 existence of vertical folds affecting little reflective monotonous lithologies also results in a
584 fairly transparent upper crust in most of the ALCUDIA section (Fig. 7).



585 None of the upper crustal reflections observed and interpreted in the presented Iberian Massif
586 NI seismic sections seems to cut across the whole crust, always rooting in a sole thrust (ESCIN-
587 1, Fig. 3) or in the lower crust (the rest of them).

588 **4.2. The lower crust in the Iberian Massif: accommodation of shortening, extension and its**
589 **nature**

590 The Iberian Massif dataset presented here shows a very coherent image of the lower crust. Its
591 reflectivity is high and usually subhorizontal. However, cross cutting relationships with later
592 features of opposite dips evidence a multi-phase origin for this reflectivity.

593 The SPZ, OMZ, WALZ, CZ and the southern CIZ show that this part of the crust is also thick (4 to
594 6 s TWT). However, in NW Iberia and the northern part of the ALCUDIA section (Figs. 1 and 7),
595 the few existing NI profiles indicate that in the northern CIZ, the lower crust is much
596 thinner (1 to 2 s TWT) and irregular (ESCIN-3.2, Figs. 6 and 9). This thin lower crust has been
597 observed in the area characterized by outcropping syn-collisional granitoids (zone II of
598 Simancas et al., 2013). These witness the onset of crustal re-equilibration processes triggered
599 by gravitational collapse, extension and crustal melting during the Late Carboniferous. The
600 straightforward conclusion is to attribute the architecture of this lower crust to late Variscan
601 orogenic extension and melting, implying that crustal thinning has been mostly accommodated
602 by its lowermost part.

603 Nevertheless, a gap of crustal-scale NI data exists in most of the northern CIZ. The CIMDEF
604 noise autocorrelation profiles (Figs. 1 and 9 and) show a thick (~5 s TWT) lower crust in most
605 of this area, which essentially corresponds to the CIZ (Andrés et al., 2019 and this volume). This
606 is in conflict with the NI sections ESCIN-3.2 and northernmost ALCUDIA, where the highly
607 reflective lower crust is less than half as thick. However, granitoids are probably scarce in the
608 Variscan basement hidden under the DB, which can then present a thick lower crust. But in
609 and near the ICS, a rather continuous internal reflection in the lower crust could be interpreted
610 as its top part (Figs. 9 and 10), thus indicating that crustal thinning and melting, observed in
611 the surface, has also affected the lower crust (Andres et al., this volume).

612 Extension in the northern CIZ occurred simultaneously with shortening in the SW Iberian
613 Massif. According to Simancas et al. (2013) this suggests that the tectonic stresses would be
614 dominantly compressional, still induced by ongoing collision. In fact, gravitational instabilities
615 in a thickened crust should mostly be affecting the upper crust. In this context, theoretical
616 models (Royden, 1996; Seyferth and Henk, 2004) indicate that beneath the areas of extension
617 in the upper crust, shortening may prevail in the lower crust. This mechanism is an efficient
618 way for syn-convergent exhumation of deep rocks.

619 Indeed, from a regional tectonic perspective, compression was active till the end of the
620 Variscan orogeny, and at times, clearly simultaneous with extension (C3 and E2 overlapped in
621 the interval 315-305 Ma; Martínez Catalán et al., 2014). But it is clear that extension affected
622 the lower crust, as it appears thinned in areas of transparent, extended molten crust (ESCIN-
623 3.2 and ALCUDIA sections, Figs. 6 and 7). However, the irregular pattern observed in the ESCIN-
624 3.2 lower crust might indicate the existence of folds in this re-equilibrated layer, witnessing the
625 simultaneity of extension and compression even at lower crustal level (Fig. 6). In addition, we



626 cannot rule out that these undulations represent boudinage (i.e. extension) or Alpine folding,
627 although we consider the latter less likely.

628 In the ALCUDIA section, the imaged part of the CIZ underwent only moderate upper crustal
629 shortening (Martínez Poyatos et al., 2012). According to Simancas et al. (2013), the thick
630 laminated lower crust, representing pre-Pennsylvanian (most probably pre-Variscan) ductile
631 deformation, appears deformed in two sectors near both ends of the profile, concentrating
632 shortening in discrete structures that compensate the upper crustal deformation. The first of
633 them is the very conspicuous crocodile-like structure observed in the southern end, and also
634 imaged in the northern part of the IBERSEIS line (Fig. 9b). This structure mimics localized
635 crustal indentation of the OMZ into the CIZ, producing a local underthrusting of the latter to
636 the S that is still (partly?) preserved. Indentation generated tectonic inversion of the Los
637 Pedroches early Carboniferous basin (Simancas et al., 2013) and bending of the overlying
638 upper crust, as seen by the uplift of the IRB, both of which predate the imbrication. The Los
639 Pedroches batholith intruded above at 314-304 Ma in an extensional setting (Carracedo et al.,
640 2009), postdating the age of the wedge as no further deformation affected the batholith.
641 Indeed, the crocodile-like feature must represent early Carboniferous Variscan compressional
642 deformation and must account for part of the shortening observed at upper crustal level.

643 However, to the NE of this section, a ramp-and-flat geometry has been interpreted as a major
644 lower crustal thrust (Martínez Poyatos et al., 2012; Simancas et al., 2013) that helps to
645 compensate upper and lower crustal shortening. However, the highly reflective lower crust is
646 not repeated in the hanging wall to the structure, so that a subtractive character is a
647 reasonable alternative. As stated above, the thin lower crust to the N of the ramp seems to be
648 clear evidence of lower crustal thinning (Fig. 9b), supported by the fact that it underlies an
649 area of upper crustal extension, the Toledo gneiss dome, characterized by normal faulting and
650 pervasive partial melting (Barbero, 1995; Hernández Enrile, 1991). Regardless of how much
651 shortening that area accommodated during crustal thickening and even though the observed
652 ramp could be a former thrust fault reactivated during later extension, the present image of
653 the lower crust does not suggest compensation of upper crustal shortening. In fact, the lower
654 crust in the ALCUDIA section is anomalously thick elsewhere (up to 6 s TWT, 18 km) suggesting
655 the possibility of ductile thickening previous to the extension that triggered thinning at its
656 northern part.

657 In the IBERSEIS profile, lower crustal dominant reflectivity is also subhorizontal but disrupted
658 by N and S dipping features (Fig. 9b). Whereas in the OMZ these features usually dip to the N,
659 as do the upper crustal reflections representing Variscan thrusts, in the SPZ they surprisingly
660 mirror the upper crustal Variscan thrusts, dipping to the S. Furthermore, one of these features,
661 placed close to the boundary with the OMZ, affects almost the entire lower crust.

662 Orogenic orthogonal shortening in the OMZ upper crust has been estimated in 120 km (~57%)
663 and in the SPZ around 80 km (~45%) or even less (Pérez-Cáceres et al., 2016). According to
664 Simancas et al. (2013), the crocodile structure and a not observed associated northward
665 subduction of the OMZ might account for this shortening in the OMZ. Similarly, in the SPZ, the
666 lower crustal imbricated structures represent only ~ 20 km of shortening so that according to



667 these authors, detached lower crustal subduction along the OMZ/SPZ might have
668 accommodated the other 60 km.

669 In this regard, we suggest that the present day SPZ crustal image represents its decoupled
670 early Carboniferous extension and later compression. This evolution would have erased any
671 evidences of previous (pre-Carboniferous) subduction, and forced the SPZ to thin during
672 extension. i.e., the lower crust had to decrease its thickness ductilely, perhaps first in a more
673 or less distributed way and later through localized shear zones (brittle or not depending on the
674 depth) as it became shallower. However, the upper crust could have preserved most of its
675 original thickness, as the developing basins associated to extension would have been
676 constantly fed by sediments and igneous extrusions and intrusions (like the IRB in the OMZ).
677 Later compression would have folded and thrust the upper crust, and also thickened the
678 lower crust. A few lower crustal normal shear zones might have developed during extension
679 and then be reactivated as ductile thrusts during compression. Those are today observed as S
680 dipping reflections that disrupt the subhorizontal previous reflectivity in the lower crust and
681 mirror thrusts in the upper crust. Accordingly, distributed ductile deformation and thrusting
682 might have thickened the lower crust back to its original (or simply stable) thickness in the SPZ
683 and elsewhere, something that cannot be measured but would need to be accounted for when
684 comparing shortening at upper and lower crustal level. The resulting seismic image of the SPZ
685 would then be that of an extended and then inverted margin, with mirroring reflectors in the
686 upper and lower crust merging in a mid-crustal discontinuity and providing a seismic image
687 different to that of a typical foreland thrust and fold belt (e.g., CZ; Fig. 3). This evolution differs
688 from that of a hyperextended magma-rich margin as stretching of the upper and lower crust is
689 not coupled and faults do not cut across the crust and penetrate down into the mantle. In any
690 case, the S dipping lower crustal reflections, active during the Late Carboniferous, postdate the
691 sub horizontal reflectivity of the lower crust. It is worth mentioning here that the SPZ seismic
692 image is identical to that of the Rhenohercynian Massif in Germany (Franke et al., 1990;
693 Oncken, 1998) suggesting a similar evolution.

694 The discussion above shows that the lower crust in the Iberian Massif is thick, except when it is
695 affected by late orogenic extension. The mechanisms that produced lower crustal thickening
696 are probably related with compressional deformation, mostly ductile. Continental
697 underthrusting of the CZ underneath the WALZ (Ayarza et al., 1998, 2004), indentation of the
698 OMZ in the CIZ (Fig. 9b) and Variscan thrust-like structures probably played an important role.
699 In addition, the latter help to constrain the age of the subhorizontal reflectivity. Frequent
700 disruption of subhorizontal lower crustal lamination by Variscan (late Carboniferous) dipping
701 features indicates that the lamination developed prior to Variscan compressional deformation.
702 What this lamination represents is still an open question.

703 Many vertical incidence seismic reflection profiles worldwide have shown reflective lower
704 crusts (e.g., Meissner et al., 2006; Wever, 1989). Lower crust seismic lamination has been
705 often related to late orogenic extensional events (Meissner, 1989). In the Iberian Massif,
706 surface geology shows that late orogenic extension affects the upper crust, mainly in areas of
707 large previous thickening. In contrast to this author's models, important thinning of the lower
708 crust takes place in those areas (ESCIN-3.2 and northern ALCUDIA, Figs. 6, 7 and 9). Certainly,
709 lower crustal lamination might come from underplating eased by extension in magma rich



710 margins (Klemperer et al., 1986). But also, ductile deformation is a very likely source of lower
711 crustal lamination. Dipping events observed in the lower crust crosscutting a strong banded
712 reflectivity represent the latest orogeny-related shortening, which will be further flattened and
713 horizontalized in the next orogeny. Continuous superposition of deformational events at lower
714 crustal level managed to decrease the dip of structural/lithological markers and define a
715 subhorizontal fabric. These deformation mechanisms can generate structures with a strongly
716 defined anisotropy, which result in a strongly laminated lower crustal fabric (Carbonell and
717 Smithson, 1991; Okaya et al., 2004). Accordingly, a laminated lower crust may represent an
718 overly reworked lower crust that has been ductilely deformed over several orogenies.
719 Opposite to the model by Meissner (1989), such a horizontal reflectivity is observed along the
720 Iberian Massif in areas where late orogenic extension is absent or weak: the SPZ (Avalonia),
721 the OMZ (peri-Gondwana), the not extended CIZ, the WALZ and the CZ (Gondwana). Thus, we
722 suggest that strong lamination in the deep crust is probably a global characteristic of reworked
723 lower crusts not affected by late orogenic extension in the latest orogeny.

724 **4.3. The Moho and crustal thickness in the Iberian Massif**

725 The crust-mantle boundary, i.e., the Moho, is basically flat in the Iberian Massif except where
726 affected by the Alpine tectonics (Fig. 10). This is rather surprising as the lower crust seems to
727 be quite well preserved, suggesting that the Moho geometry has been flattened out through
728 slow, not invasive, readjustments.

729 Flat Mohos imply the existence of either isostatic and/or thermal, late to post-orogenic
730 processes that have managed to eliminate crustal roots (Cook, 2002). NW Iberia was affected
731 by late Carboniferous extension that heated and reworked the CIZ, possibly without significant
732 mantle involvement (Alcock et al., 2009, 2011), but producing crustal thinning (Palomeras et
733 al., 2017: see Moho depth map in Fig. 10). Thick and thermally mature crusts might experience
734 lateral flow of its low-viscosity deeper part that contributed to reduce crustal roots (Seyferth
735 and Henk, 2004). This process might have partly occurred in the CIZ sampled by the ESCIN-3.2
736 section (Fig. 6) where an outstanding change in lower crustal thickness and signature exist,
737 manifested by a thinner and very reflective lower crust in contrast to that to the E, in the WALZ
738 (1 vs 3 s TWT). In the latter, the Variscan crust is still thick even though it experienced late-
739 Variscan extension in its western part and the whole area was slightly affected offshore by the
740 extension linked to the opening of the Bay of Biscay.

741 In the SW Iberian Massif, a thick laminated lower crust is still observable while the Moho depth
742 is fairly constant (~10s TWT). Carboniferous-to-Permian isostatic rebound in response to
743 tectonic thickening, erosion and localized Permian thermal readjustments must have
744 contributed to flatten the Moho. However, seismic reflections show that crustal imbrication
745 into the mantle has locally survived post-orogenic Moho resetting. This indicates that isostatic
746 equilibrium has been reached in a long wavelength scale, but that local features can still
747 remain if they can be supported by the crustal strength and do not pose an isostatic constraint.

748 **4.4. The (missing) middle crust in the Iberian Massif (and elsewhere?)**

749 One of the highlights of this work is the lack of a seismic layer that can be identified with the
750 middle crust. But, what is the middle crust?



751 From a metamorphic point of view, the middle crust could be ascribed to the mesozone, which
752 may be correlated with the amphibolite facies, whose temperature ranges between 400-500
753 and 600-800°C, the precise limits depending on the pressure (Spear, 1993). In addition, the
754 epizone, between 200-250 and 400-500°C and typically represented by the greenschist facies,
755 is also a metamorphic entity which develops during metamorphism under several kilometers
756 of anchi- and no metamorphic rocks. The depths corresponding to these temperature intervals
757 vary with the geothermal gradient. For a Barrovian gradient, typical of a continental crust
758 undergoing collision, the depths for epizone and mesozone can be estimated around 10-20
759 and 20-30 (± 5) km respectively. However, the boundaries of these metamorphic zones might
760 have a gravity, i.e. density signature, but not a seismic one. Furthermore, epi-, meso- and
761 catazonal rocks outcrop everywhere in any eroded orogenic belt, implying that they do not
762 represent a seismic mid crust but actually occur in the upper crust.

763 From a seismic point of view, a middle crust could be a crustal level bounded in its upper and
764 lower parts by characteristic reflections that indicate the existence of important impedance
765 contrasts at its top and bottom. In this regard, only the IRB, intruded between the upper and
766 the lower crust (Carbonell et al., 2004; Simancas et al., 2003), and providing conspicuous
767 velocity contrasts (Palomeras et al., 2009, 2011) fulfill that requirement. However, it is most
768 probably an intrusion emplaced at a mid-crustal discontinuity and does not represent the
769 middle crust.

770 WA reflection seismic data from the northern Iberian Massif have often resulted in
771 multilayered models despite weak evidences of continuous reflectivity at these levels (Ayarza
772 et al., 1998; Fernández-Viejo et al., 1998, 2000; Pedreira et al., 2003). Even though local
773 velocity contrasts capable of providing weak and patchy reflectivity contrasts exist at different
774 crustal depths (e.g., thrust faults and normal detachments may represent lithological
775 boundaries with a noticeable velocity contrast), these are not orogen-scale features but local
776 reflectors. Many of these reflections observed, interpreted and/or extrapolated as middle
777 crust in seismic WA datasets belong in fact to the upper crust, when compared with NI data,
778 i.e., lie above the mid-crustal discontinuity. In this regard, the short wavelength
779 heterogeneities of the crust can be seen by low resolution WA dataset as laterally continuous
780 features (Levander and Holliger, 1992), something that has led us to wrong models.

781 According to the above we argue that, in the Iberian Massif, no seismic middle crust can be
782 identified. In the hinterland, reflectors imaging deformation in the upper crust root in the top
783 of the lower crust. Only in ESCIN-1, which depicts the thin-skinned deformation of the CZ,
784 thrust faults root in a sole thrust and one could argue that the basement underneath these
785 shallow reflections represents the middle crust. But in the shallower part, to the E, early
786 Paleozoic and Neoproterozoic sediments occur on both sides of the sole thrust. Also, in the
787 deeper parts, to the W, the previous crystalline basement is probably involved in imbrications
788 affecting the upper crust. Thus, in our opinion, that non-reflective basement represents the
789 upper crust.

790 In the Iberian Massif, the Paleozoic was deposited unconformably above Neoproterozoic
791 sediments which could be considered as its basement, but these were not metamorphic then.
792 Only in the OMZ, greenschist to amphibolite facies Neoproterozoic represents the Cadomian



793 basement, but it cannot be distinguished from the overlying Paleozoic metasediments in the NI
794 profiles. An even older crystalline basement of felsic composition exists, as indicated by
795 inherited zircons of 830-2000 Ma found in Ediacaran orthogneisses, Lower Ordovician
796 volcanics and Variscan granitoids that resulted from partial melting of such a basement
797 (Fernández-Suárez et al., 1998; Montero et al., 2007; Villaseca et al., 2012). Again, its upper
798 boundary is not imaged on NI profiles. These data also suggest that, in the Iberian Massif,
799 there are no crustal intervals that can be related with a seismic middle crust. Decoupling of
800 reflectivity, i.e. deformation, at a mid-crustal level define just an upper and a lower crust.

801 **4.5. Significance of a mid-crustal discontinuity: the Conrad discontinuity?**

802 Inspection of the Iberian Massif NI seismic dataset leads us to conclude that an orogenic-scale
803 mid-crustal discontinuity exists. This surface does not always provide a clear reflection, as in the
804 SPZ, but it is clearly defined by the geometry of the upper and lower crustal reflections,
805 asymptotically merging into it. The discontinuity coincides with the top of the lower crust,
806 which is often much more reflective than the upper crust. Furthermore, this discontinuity has
807 probably acted as a detachment for Variscan deformation in the hinterland of the orogen and
808 in the SPZ. However, in the CZ, the transition between upper and lower crust is poorly defined,
809 in accordance with the fact that its basement was not affected by Variscan tectonics. There, a
810 detachment level interpreted as the sole thrust of the thin-skinned wedge occurs above the
811 lower crust, and no deformation decoupling is identified above or below this feature.

812 Simancas et al. (2013) already described this discontinuity on the basis of the asymptotic
813 geometry of the SPZ faults towards the middle of the crust. These authors concluded that its
814 depth greatly varies when reaching suture boundaries, where the discontinuity roots. Although
815 we do not observe a subduction zone in the reworked elusive suture between the SPZ and the
816 OMZ (Pérez-Cáceres et al., 2015), and interpret the OMZ/CIZ suture as an indentation between
817 two continental crusts, triggering imbrication into the mantle of the latter (crocodile
818 structure), we agree that this discontinuity would have eased the decoupling of the Iberian
819 crust, allowing subduction of its lower part while the upper part was deformed by folds and
820 thrust faults. This is clearly observed in the Alpine northward subduction of the Iberian Massif
821 lower crust underneath the CZ (ESCIN-2, Fig. 4) and also, in the Pyrenees, where a detached
822 Iberian lower crust subducts to the N (Teixell et al., 2018). In the Iberian Massif, the complexity
823 of Variscan tectonics and late-Variscan crustal re-equilibration has mostly removed evidences
824 of a such mechanisms, but a comparable example has been preserved in the NW: the thick
825 lower crust imaged by ESCIN-3.3 is interpreted as underthrusting of the CZ lower crust under
826 that of the WALZ (Ayarza et al., 1998; Martínez Catalán et al., 2003, 2012, 2014).

827 The mid crustal discontinuity has been interpreted as the brittle-ductile transition (e.g. Ehsan
828 et al., 2014; Simancas et al., 2013). Indeed, it bounds a lower crust, highly reflective and
829 ductilely deformed from the upper crust. However, Variscan ductile deformation occurs also
830 above the discontinuity and is a general feature of the whole Iberian Massif except for the CZ.
831 If we deal with present deformation mechanisms, it is unlikely that the brittle-ductile
832 transition, which depends on the values of P and T, coincide with the described discontinuity,
833 because, i) it does not necessarily imply an impedance contrast (Litak and Brown, 1989), and
834 ii) according to figure 10, the depth of the discontinuity varies from 4 s TWT (~12 km, ALCUDIA



835 section) to 8 s TWT (~24 km, ESCIN-2 section) which would imply unrealistic variations on P
836 and T in the present crust.

837 The Iberian laminated lower crust is probably very old. Granulites dredged in Mesozoic
838 sediments of the Cantabrian margin have yielded ages of up to 1400 Ma (Capdevila et al., 1980
839 and references therein). Even older values have been obtained for granulites from the Galicia
840 Bank (Gardien et al., 2000), which featured Ar-Ar ages of up to 2500 Ma. These granulites have
841 been deformed ductilely during several orogenies. Rocks lying above the lower crust, whatever
842 their nature is, are separated from it by a discontinuity that fosters decoupled deformation
843 between both crustal layers. Accordingly, we think that the observed mid-crustal discontinuity
844 represents a rheological boundary that separates rocks that have been deformed differently.
845 The boundary, located at the top of the lower crust, represents a velocity contrast as the latter
846 is probably composed of dense granulites and includes relatively abundant basic rocks, which
847 makes it easily identifiable in seismic sections.

848 The geometry of this discontinuity and its depth, together with that of the Moho (Fig. 10),
849 provide insights of the evolution of the Iberian Massif. Along the SW Iberian Massif, the mid-
850 crustal discontinuity is sub-horizontal and lies at a depth between 4-6 s TWT. In the OMZ, the
851 intrusion of the IRB allows to establish its depth in the top or the bottom of this feature, but in
852 average, its location would fit the above given values. However, in the centre and NW, the
853 position of the discontinuity varies, deepening down to 8 s TWT (Figs. 9 and 10).

854 The low resolution noise autocorrelation models obtained along the CIMDEF profile shows
855 confusing results along the central Iberian Massif. In central Iberia, the mid-crustal
856 discontinuity might lie at 5-6 s TWT, deepening around the ICS to 8 s TWT as it has been
857 affected by pervasive extension and melting, thus defining a thin lower crust (2 s TWT, ~6 km,
858 Figs. 9 and 10). Accordingly, this feature appears redefined in this area, and now follows the
859 geometry of the ICS batholith. The change in the depth and geometry of this discontinuity and
860 the thinning of the lower crust might have allowed coupled deformation, letting part of the
861 upper crust to the S of the ICS to underthrust it (Andrés et al. this volume). This would foster
862 the 400-500 m topographic change between the N and S foreland basins of this Alpine
863 mountain range (Fig. 9). In fact, Simancas et al. (2013) argues that coupled crustal deformation
864 takes place when a relatively weak lower crust exists something that might well represent the
865 context of the ICS. The resulting geometry of this Alpine reactivation and its topographic
866 imprint is different to that observed to the N, in the CZ, where late orogenic extension and
867 melting does not exist and the mid-crustal discontinuity has been preserved. On the other
868 hand, the lower crust imaged along the CIMDEF transect presents a conspicuous internal
869 reflection that could also be interpreted as the top of the lower crust. If this were the case, the
870 lower crust would be even thinner along the entire section, matching the characteristics
871 observed to the N of the ALCUDIA section and in the ESCIN-3.2 line. In any case, we argue that
872 the mid-crustal discontinuity and the lower crust we are seeing in the CIMDEF profile are both
873 probably reworked by extension but not totally re-equilibrated and thus, its seismic image is
874 confusing. Moho depth models (Fig. 10) derived from shear wave tomography (Palomeras et
875 al., 2017) indicate that along the CIMDEF profile the crust is thin (except in the Alpine root) but
876 not as much as in NW Iberia, so that lower crustal extension and re-equilibration may have not
877 been as intense as in the GTMZ and CIZ of the NW Iberian Massif.



878 The most outstanding change in the mid-crustal discontinuity architecture appears in NW
879 Iberia along the ESCIN-3.2 profile. This section features the thinnest crust (9 s TWT)
880 accompanied by the thinnest lower crust (~1 s TWT). The mid-crustal discontinuity lies at 8 s
881 TWT in contrast to the depth where it appears in the neighbouring ESCIN-3-3 and ESCIN-1
882 lines, where it is located between 6 and 8 s TWT, suggesting that it has been redefined.
883 Nevertheless, clear reflections root in its upper part indicating that it still acted as a
884 discontinuity/detachment. The depth of this feature in the NW corner of Iberia is similar to
885 that of the high amplitude lower crustal internal reflection near the ICS. Accordingly, we
886 suggest that in NW Iberia, gravitational collapse followed by crustal melting and extension has
887 thinned the crust (Fig. 10), and specially the lower crust, relocating the mid-crustal
888 discontinuity.

889 NW Iberia was importantly thickened (up to 50-70 km) due to the emplacement of the GTMZ
890 allochthonous complexes. Thermal models by Alcock et al. (2009, 2015) show that as a result
891 the upper mantle continued increasing its temperature 60-65 Ma after the start of
892 compressional deformation at 360 Ma. This implies large thinning of the mantle lithosphere,
893 from 70 to 25-30 km, due to the ascent of the 1300 °C isotherm. It is not surprising that the
894 lower crust there became the most extended as a consequence of the heat increase, as in the
895 models it reached 800 °C after 45 Ma and 900 °C after 55 Ma (315-305 Ma).

896 The idea of a mid-crustal velocity discontinuity was put forward in the 1920's (Conrad, 1925).
897 Early analysis of natural source earthquake recordings and later images from controlled source
898 seismic reflection data provided further evidences that supported a clear distinction between
899 upper and lower crust. These evidences led to considering the Conrad discontinuity, a global
900 scale feature present the continental crust. However, this was later challenged as some results
901 of deep seismic reflection profiling did not show a clear distinction between upper and lower
902 crust (Litak and Brown, 1989).

903 Mid-crustal discontinuities have, however, been observed very often and in different types of
904 seismic data worldwide (e.g., Fianco et al., 2019; Hobbs et al., 2004; Melekhova et al., 2019;
905 Oncken, 1998; Ross et al., 2004; Snelson et al., 2013). Important changes in the rheology of the
906 crust have also been reported at those depths (Maggini and Caputo, 2020; Wever, 1989)
907 supporting the idea that a mechanical boundary must exist. Thus, we suggest that, even
908 though it is not observed everywhere (Litak and Brown, 1989), this feature is an orogen-scale,
909 world class crustal continental discontinuity (Artemieva, 2009), often coinciding with the top of
910 the highly laminated lower crust (when there is one). Its existence might determine the way
911 the crust deforms, easing decoupled deformation. Orogenic evolution, i.e. rifting, extension,
912 melting, etc. may modify it or even erase it, thus its existence and geometry might help us to
913 understand the geologic history of continents. In this regard, and coming back to the long-
914 forgotten discussion of the nature of the Conrad discontinuity (Conrad, 1925) and its position
915 on top of the laminated lower crust (Wever, 1989), we suggest that, in the Iberian Massif, the
916 observed mid-crustal feature fulfills the characteristics of this debated discontinuity. Its clear
917 signature and regional extension contributes to unravel its nature and significance.

918 **5. Conclusions**



919 Normal incidence seismic data acquired across the Iberian Massif in the last 30 years have
920 provided an entire section of a well exposed and almost complete part of the European
921 Variscides. Existing gaps in the central part have been recently sampled by passive source
922 seismic recordings (noise and earthquakes) that provide fairly good constraints on the crustal
923 structure.

924 Results show that crustal thickness varies from ~9 s TWT in late-Variscan extended areas (NW
925 of the Central Iberian Zone), to ~10 s TWT (30-33 km) in the external South Portuguese Zone to
926 ~12 s TWT (36-38 km) in the internal West Asturian-Leonese Zone. Alpine reactivation has
927 managed to further thicken the crust to at least ~14 s TWT (42-45 km) in the external
928 Cantabrian Zone and to 35-38 km in the Iberian Central System, a Tertiary orogenic belt
929 developed in Central Spain. The top of a thick (up to 6 s TWT) and very reflective lower crust
930 helps to define a mid-crustal discontinuity across the entire Iberian Massif. This boundary
931 represents a level where reflections from the upper and lower crust merge asymptotically,
932 thus suggesting that it has often acted as a detachment or a decoupling level. Its position and
933 geometry varies mostly in relation to the late Variscan evolution. Accordingly, it is deeper in
934 NW and central Iberia (~8 s TWT), where Variscan crustal thickening was important and
935 gravitational collapse melted and extended the crust, thus defining a very thin lower crust.
936 However, it appears between 4-6 s TWT to the SW, where the crust did not thicken as much
937 and its original structure is better preserved, being later re-equilibrated through slow isostasy
938 and erosion.

939 This discontinuity exists in all the Iberian Massif tectonic zones, regardless of their Gondwana
940 or Avalonia affinity, thus suggesting it is an orogenic-scale discontinuity. We interpret it as the
941 rheological boundary between an overly ductilely deformed old lower crust and a
942 heterogeneous variably (often also ductilely) deformed upper crust that mostly (but not only)
943 shows evidences of the latest orogenic event. Its geometry, position and extent match the
944 characteristics defined for the long-forgotten Conrad discontinuity. The identification of similar
945 features in normal incidence profiles worldwide supports its inclusion as a major crustal
946 discontinuity.

947 **Acknowledgements**

948 The seismic data was reprocessed using the commercial seismic signal processing software
949 Claritas. Funding for this research was provided by the Junta de Castilla y León (SA065P17), the
950 Spanish Ministry of Science and Innovation (CGL2016-78560-P) and the Generalitat de
951 Catalunya (grant 2017SGR1022).

952 **References**

953 Alcock, J. E., Martínez Catalán, J. R., Arenas, R. and Díez Montes, A.: Use of thermal modeling
954 to assess the tectono-metamorphic history of the Lugo and Sanabria gneiss domes, Northwest
955 Iberia, *Bull. la Soc. Geol. Fr.*, 180(3), 179–197, doi:10.2113/gssgfbull.180.3.179, 2009.

956 Alcock, J. E., Martínez Catalán, J. R. and Arenas, R.: One- and two-dimensional models are
957 equally effective in monitoring the crust's thermal response to advection by large-scale
958 thrusting during orogenesis, *Comput. Geosci.*, 37(8), 1205–1207,
959 doi:10.1016/j.cageo.2011.02.012, 2011.



- 960 Alcock, J. E., Martínez Catalán, J. R., Rubio Pascual, F. J., Díez Montes, A., Díez Fernández, R.,
961 Gómez Barreiro, J., Arenas, R., Dias da Silva, Í. and González Clavijo, E.: 2-D thermal modeling
962 of HT-LP metamorphism in NW and Central Iberia: Implications for Variscan magmatism,
963 rheology of the lithosphere and orogenic evolution, *Tectonophysics*, 657, 21–37,
964 doi:10.1016/j.tecto.2015.05.022, 2015.
- 965 Alonso, J. L., Marcos, A. and Suárez, A.: Paleogeographic inversion resulting from large out of
966 sequence breaching thrusts: The León Fault (Cantabrian zone, NW Iberia). A new picture of the
967 external Variscan thrust belt in the Ibero-Armorican arc, *Geol. Acta*, 7(4), 451–473,
968 doi:10.1344/105.000001449, 2009.
- 969 Álvarez-Marrón, J., Pérez-Estaún, A., Dañobeitia, J. J., Pulgar, J. A., Martínez Catalán, J. R.,
970 Marcos, A., Bastida, F., Ayarza, P., Aller, J., Gallart, A., González-Lodeiro, F., Banda, E., Comas,
971 M. C. and Córdoba, D.: Seismic structure of the northern continental margin of Spain from
972 ESCIN deep seismic profiles, *Tectonophysics*, 264, 153–174, doi:10.1016/S0040-
973 1951(96)00124-2, 1996.
- 974 Andrés, J., Draganov, D., Schimmel, M., Ayarza, P., Palomeras, I., Ruiz, M. and Carbonell, R.:
975 Lithospheric image of the Central Iberian Zone (Iberian Massif) using global-phase seismic
976 interferometry, *Solid Earth*, 10(6), 1937–1950, doi:10.5194/se-10-1937-2019, 2019.
- 977 Arenas, R., Farias, P., Gallastegui, G., Gil Ibaguchi, I., González Lodeiro, F., Klein, E., Marquínez,
978 J., Martín Parra, L. M., Martínez Catalán, J. R., Ortega, E., de Pablo Maciá, J. G., Peinado, M. and
979 Rodríguez Fernández, L. R.: Características geológicas y significado de los dominios que
980 componen la Zona de Galicia-Trás-os- Montes. Simposio sobre Cinturones Orogénicos, in
981 Simposio sobre Cinturones Orogénicos. II congreso Geológico de España, pp. 75–84, SGE., 1988.
- 982 Arenas, R., Martínez Catalán, J. R., Martínez Sánchez, S., Díaz García, F., Abati, J., Fernández-
983 Suárez, J., Andonaegui, P. and Gómez-Barreiro, J.: Paleozoic ophiolites in the Variscan suture of
984 Galicia (northwest Spain): Distribution, characteristics, and meaning, *Mem. Geol. Soc. Am.*,
985 200(22), 425–444, doi:10.1130/2007.1200(22), 2007.
- 986 Artemieva, I.: Continental Crust, *Geophysics and Geochemistry Vol.II -Encyclopedia of Earth
987 and Atmospheric Sciences in the Global Encyclopedia of Life Support Systems*, UNESCO., 2009.
- 988 Ayarza, P., Martínez Catalán, J. R., Gallart, J., Pulgar, J. A. and Dañobeitia, J. J.: Estudio Sísmico
989 de la Corteza Ibérica Norte 3 . 3 : A seismic image of the Variscan crust in the hinterland of the
990 NW Iberian Massif, *Tectonics*, 17(2), 171–186, 1998.
- 991 Ayarza, P., Martínez Catalán, J. R., Alvarez-Marrón, J., Zeyen, H. and Juhlin, C.: Geophysical
992 constraints on the deep structure of a limited ocean-continent subduction zone at the North
993 Iberian Margin, *Tectonics*, 23(1), doi:10.1029/2002TC001487, 2004.
- 994 Azor, A., Lodeiro, F. G. and Simancas, J. F.: Tectonic evolution of the boundary between the
995 Central Iberian and Ossa-Morena zones (Variscan belt, southwest Spain), *Tectonics*, 13(1), 45–
996 61, doi:10.1029/93TC02724, 1994.
- 997 Azor, A., Rubatto, D., Simancas, J. F., González Lodeiro, F., Martínez Poyatos, D., Martín Parra,
998 L. M. and Matas, J.: Rheic Ocean ophiolitic remnants in southern Iberia questioned by SHRIMP
999 U-Pb zircon ages on the Beja-Acebuches amphibolites, *Tectonics*, 27(5), 1–11,
1000 doi:10.1029/2008TC002306, 2008.
- 1001 Bandrés, A., Eguíluz, L., Pin, C., Paquette, J. L., Ordóñez, B., Le Fèvre, B., Ortega, L. A. and Gil
1002 Ibaguchi, J. I.: The northern Ossa-Morena Cadomian batholith (Iberian Massif): Magmatic arc



- 1003 origin and early evolution, *Int. J. Earth Sci.*, 93(5), 860–885, doi:10.1007/s00531-004-0423-6,
1004 2004.
- 1005 Barbero, L.: Granulite-facies metamorphism in the Anatectic Complex of Toledo, Spain: late
1006 Hercynian tectonic evolution by crustal extension, *J. Geol. Soc. London*, 152(2), 365–382,
1007 doi:10.1144/gsjgs.152.2.0365, 1995.
- 1008 BIRPS, B. I. R. P. S. and ECORS, E. de la C. C. et O. par R. et R. S.: Deep seismic reflection
1009 profiling between England, France and Ireland., *J. - Geol. Soc.*, 143(1), 45–52,
1010 doi:10.1144/gsjgs.143.1.0045, 1986.
- 1011 Bortfeld, R. K.: First results and preliminary interpretation of deep- reflection seismic
1012 recordings along profile DEKORP 2-South (FRG)., *J. Geophys. - Zeitschrift fur Geophys.*, 57(3),
1013 137–163, 1985.
- 1014 Braid, J. A., Brendan Murphy, J., Quesada, C. and Mortensen, J.: Tectonic escape of a crustal
1015 fragment during the closure of the Rheic Ocean: U-Pb detrital zircon data from the late
1016 Palaeozoic Pulo do Lobo and South Portuguese zones, Southern Iberia, *J. Geol. Soc. London.*,
1017 168(2), 383–392, doi:10.1144/0016-76492010-104, 2011.
- 1018 Braid, J. A., Murphy, J. B., Quesada, C., Bickerton, L. and Mortensen, J. K.: Probing the
1019 composition of unexposed basement, South Portuguese Zone, southern Iberia: Implications for
1020 the connections between the Appalachian and Variscan orogens, *Can. J. Earth Sci.*, 49(4), 591–
1021 613, doi:10.1139/E11-071, 2012.
- 1022 Capdevila, R., Boillot, G., Lepvrier, C., Malod, J. A. and Mascle, G.: Les formations cristallines du
1023 Banc Le Danois (marge nord-ibérique), *CR Acad. Sci. Paris, D*, 291(January), 317–320 [online]
1024 Available from:
1025 [http://scholar.google.com/scholar?hl=en&btnG=Search&q=intitle:Les+formations+cristallines+
1026 du+Banc+Le+Danois+\(marge+nord+ibérique\)#0](http://scholar.google.com/scholar?hl=en&btnG=Search&q=intitle:Les+formations+cristallines+du+Banc+Le+Danois+(marge+nord+ibérique)#0), 1980.
- 1027 Carbonell, R. and Smithson, S. B.: Large-scale anisotropy within the crust in the Basin and
1028 Range province, *Geology*, 19(July), 698–701, doi:doi:10.1130/0091-7613(1991)019, 1991.
- 1029 Carbonell, R., Simancas, J. F., Juhlin, C., Pous, J., Pérez-Estaún, A., Gonzalez-Lodeiro, F., Munoz,
1030 G., Heise, W. and Ayarza, P.: Geophysical evidence of a mantle derived intrusion in SW Iberia,
1031 *Geophys. Res. Lett.*, 31(11), 1–4, 2004.
- 1032 Carracedo, M., Paquette, J. L., Alonso Olazabal, A., Santos Zalduegui, J. F., de García de
1033 Madinabeitia, S., Tiepolo, M. and Gil Ibarguchi, J. I.: U-Pb dating of granodiorite and granite
1034 units of the Los Pedroches batholith. Implications for geodynamic models of the southern
1035 Central Iberian Zone (Iberian Massif), *Int. J. Earth Sci.*, 98(7), 1609–1624, doi:10.1007/s00531-
1036 008-0317-0, 2009.
- 1037 Carvalho, D.: The metallogenetic consequences of plate tectonics and the upper Paleozoic
1038 evolution of southern Portugal, *Estud. Notas e Trab. S.F.M.*, 20(3–4), 297–320, 1972.
- 1039 Casquet, C., Galindo, C., Tornos, F., Velasco, F. and Canales, A.: The Aguablanca Cu-Ni ore
1040 deposit (Extremadura, Spain), a case of synorogenic orthomagmatic mineralization: Age and
1041 isotope composition of magmas (Sr, Nd) and ore (S), *Ore Geol. Rev.*, 18(3–4), 237–250,
1042 doi:10.1016/S0169-1368(01)00033-6, 2001.
- 1043 Chopra, S. and Alexeev, V.: Application of texture attribute analysis to 3D seismic data, *Soc.*
1044 *Explor. Geophys. - 75th SEG Int. Expo. Annu. Meet. SEG 2005*, 30(7), 767–770,
1045 doi:10.1190/1.2144439, 2005.



- 1046 Conrad, V.: Laufzeitkurven des Tauernbens vom 28, Mitt. Erdb. Komm. Wlen Akad. Wiss., 59, 1,
1047 1925.
- 1048 Cook, F. A.: Fine structure of the continental reflection Moho, Bull. Geol. Soc. Am., 114(1), 64–
1049 79, doi:10.1130/0016-7606(2002)114<0064:FSOTCR>2.0.CO;2, 2002.
- 1050 Corretgé, L. G. and Suárez, O.: Cantabrian and Palentian Zones. Igneous Rocks, in Pre-Mesozoic
1051 Geology of Iberia, edited by R. D. DAllmeyer and E. Martínez García, pp. 72–79, Srpinge-
1052 Verlag, Berlin., 1990.
- 1053 Dallmeyer, R. D. and Quesada, C.: Cadomian vs. Variscan evolution of the Ossa-Morena zone
1054 (SW Iberia): field and 40Ar/39Ar mineral age constraints, Tectonophysics, 216(3–4), 339–364,
1055 doi:10.1016/0040-1951(92)90405-U, 1992.
- 1056 Dallmeyer, R. D., Martínez Catalán, J. R., Arenas, R., Gil Iburguchi, J. I., Gutiérrez-Alonso, G.,
1057 Farias, P., Bastida, F. and Aller, J.: Diachronous Variscan tectonothermal activity in the NW
1058 Iberian Massif: Evidence from 40Ar/39Ar dating of regional fabrics, Tectonophysics, 277(4),
1059 307–337, doi:10.1016/S0040-1951(97)00035-8, 1997.
- 1060 DEKORP Research Group: Results of deep reflection seismic profiling in the Oberpfalz (Bavaria),
1061 Geophys. J. R. Astron. Soc., 89(1), 353–360, doi:10.1111/j.1365-246X.1987.tb04430.x, 1987.
- 1062 Dias, R. and Ribeiro, A.: The Ibero-Armorican Arc: A collision effect against an irregular
1063 continent?, Tectonophysics, 246(1–3), 113–128, doi:10.1016/0040-1951(94)00253-6, 1995.
- 1064 Díaz Azpiroz, M., Fernández, C., Castro, A. and El-Biad, M.: Tectonometamorphic evolution of
1065 the Aracena metamorphic belt (SW Spain) resulting from ridge-trench interaction during
1066 Variscan plate convergence, Tectonics, 25(1), 1–20, doi:10.1029/2004TC001742, 2006.
- 1067 Díez-Montes, A., Martínez Catalán, J. R. and Bellido Mulas, F.: Role of the Ollo de Sapo massive
1068 felsic volcanism of NW Iberia in the Early Ordovician dynamics of northern Gondwana,
1069 Gondwana Res., 17(2–3), 363–376, doi:10.1016/j.gr.2009.09.001, 2010.
- 1070 Díez Balda, M. A.: El Complejo Esquistos-Grauvaquico, las series Paleozoicas y la estructura
1071 Hercinica al sur de Salamanca, Universidad de Salamanca., 1986.
- 1072 Díez Balda, M. A., Martínez Catalán, J. R. and Ayarza, P.: Syn-collisional extensional collapse
1073 parallel to the orogenic trend in a domain of steep tectonics: the Salamanca Detachment Zone
1074 (Central Iberian Zone, Spain), J. Struct. Geol., 17(2), 163–182, doi:10.1016/0191-
1075 8141(94)E0042-W, 1995.
- 1076 Díez Montes, A., Martínez Catalán, J. R. and Bellido Mulas, F.: Role of the Ollo de Sapo massive
1077 felsic volcanism of NW Iberia in the Early Ordovician dynamics of northern Gondwana,
1078 Gondwana Res., 17(2–3), 363–376, doi:10.1016/j.gr.2009.09.001, 2010.
- 1079 Ehsan, S. A., Carbonell, R., Ayarza, P., Martí, D., Pérez-Estaún, A., Martínez-Poyatos, D. J.,
1080 Simancas, J. F., Azor, A. and Mansilla, L.: Crustal deformation styles along the reprocessed deep
1081 seismic reflection transect of the Central Iberian Zone (Iberian Peninsula), Tectonophysics, 621,
1082 159–174, doi:10.1016/j.tecto.2014.02.014, 2014.
- 1083 Ehsan, S. A., Carbonell, R., Ayarza, P., Martí, D., Martínez Poyatos, D., Simancas, J. F., Azor, A.,
1084 Ayala, C., Torné, M. and Pérez-Estaún, A.: Lithospheric velocity model across the Southern
1085 Central Iberian Zone (Variscan Iberian Massif): The ALCUDIA wide-angle seismic reflection
1086 transect, Tectonics, 34(3), 535–554, doi:10.1002/2014TC003661, 2015.



- 1087 Expósito, I., Simancas, J. F. and Lodeiro, F. G.: Estructura de la mitad septentrional de la zona
1088 de Ossa-Morena: Deformación en el bloque inferior de un cabalgamiento cortical de evolución
1089 compleja: Deformación en el bloque inferior de un cabalgamiento cortical de evolución
1090 compleja, *Rev. la Soc. Geológica Española*, 15(1), 3–14, 2002.
- 1091 Expósito, I., Simancas, J. F., González Lodeiro, F., Bea, F., Montero, P. and Salman, K.:
1092 Metamorphic and deformational imprint of Cambrian - Lower Ordovician rifting in the Ossa-
1093 Morena Zone (Iberian Massif, Spain), *J. Struct. Geol.*, 25(12), 2077–2087, doi:10.1016/S0191-
1094 8141(03)00075-0, 2003.
- 1095 Farias, P., Gallastegui, G., González Lodeiro, F., Marquinez, J., Martín-Parra, L. M., Martínez
1096 Catalán, J. R. and Pablo-Maciá, J. G.: “Aportaciones al conocimiento de la litoestratigrafía y
1097 estructura de Galicia Central,” *Memórias da Fac. Ciências, Univ. do Porto*, 1(January 1987),
1098 411–431, 1987.
- 1099 De Felipe, I., Pedreira, D., Pulgar, J. A., van der Beek, P. A., Bernet, M. and Pik, R.: Unraveling
1100 the Mesozoic and Cenozoic Tectonothermal Evolution of the Eastern Basque-Cantabrian Zone–
1101 Western Pyrenees by Low-Temperature Thermochronology, *Tectonics*, 38(9), 3436–3461,
1102 doi:10.1029/2019TC005532, 2019.
- 1103 De Felipe, I., Alcalde, J., Ivandic, M., Martí, D., Ruíz, M., Marzán, I., Díaz, J., Ayarza, P.,
1104 Palomeras, I., Fernández Turiel, J. L., Molina Fernández, C., Bernal, I., Brown, L., Roberts, R. and
1105 Carbonell, R.: Reassessing the lithosphere: SeisDARE, an open access seismic data repository,
1106 *Earth Syst. Sci. Data*, under rev., 2020.
- 1107 Fernández-Suárez, J., Gutiérrez-Alonso, G., Jenner, G. A. and Jackson, S. E.: Geochronology and
1108 geochemistry of the Pola de Allande granitoids (northern Spain): their bearing on the
1109 Cadomian-Avalonian evolution of northwest Iberia, *Can. J. Earth Sci.*, 35(12), 1439–1453,
1110 doi:10.1139/cjes-35-12-1439, 1998.
- 1111 Fernández-Viejo, G., Gallart, J., Pulgar, J. A., Gallastegui, J., Dañoibeitia, D. and Córdoba, D.:
1112 Crustal transition between continental and oceanic domains along the North Iberian margin
1113 from wide angle seismic and gravity data, *Geophys. Res. Lett.*, 25(23), 4249–4252, 1998.
- 1114 Fernández-Viejo, G., Gallart, J., Pulgar, A., Córdoba, D. and Dañoibeitia, J. J.: Seismic signature
1115 of Variscan and Alpine tectonics in NW Iberia: Crustal structure of the Cantabrian Mountains
1116 and Duero Basin, *J. Geophys. Res.*, 105(1999), 3001–3018, 2000.
- 1117 Fianco, C. B., França, G. S., Albuquerque, D. F., Vilar, C. da S. and Argollo, R. M.: Using the
1118 receiver function for studying earth deep structure in the Southern Borborema Province, *J.*
1119 *South Am. Earth Sci.*, 94(April), 102221, doi:10.1016/j.jsames.2019.102221, 2019.
- 1120 Finlayson, D. M., Collins, C. D. N. and Lock, J.: P-wave velocity features of the lithosphere under
1121 the Eromanga Basin, Eastern Australia, including a prominent MID-crustal (Conrad?)
1122 discontinuity, *Tectonophysics*, 101(3–4), 267–291, doi:10.1016/0040-1951(84)90117-3, 1984.
- 1123 Flecha, I., Palomeras, I., Carbonell, R., Simancas, J. F., Ayarza, P., Matas, J., González-Lodeiro, F.
1124 and Pérez-Estaún, A.: Seismic imaging and modelling of the lithosphere of SW-Iberia,
1125 *Tectonophysics*, 472(1–4), 148–157, doi:10.1016/j.tecto.2008.05.033, 2009.
- 1126 Franke, W.: The mid-European segment of the Variscides: Tectonostratigraphic units, terrane
1127 boundaries and plate tectonic evolution, *Geol. Soc. Spec. Publ.*, 179, 35–56,
1128 doi:10.1144/GSL.SP.2000.179.01.05, 2000.
- 1129 Franke, W., Bortfeld, R. K., Brix, M., Drozdowski, G., Dürbaum, H. J., Giese, P., Janoth, W.,



- 1130 Jödicke, H., Reichert, C., Scherp, A., Schmoll, J., Thomas, R., Thünker, M., Weber, K., Wiesner,
1131 M. G. and Wong, H. K.: Crustal structure of the Rhenish Massif: results of deep seismic
1132 reflection lines Dekorp 2-North and 2-North-Q, *Geol. Rundschau*, 79(3), 523–566,
1133 doi:10.1007/BF01879201, 1990.
- 1134 Gallastegui, J., Pulgar, J. A. and Alvarez-Marrón, J.: 2-D seismic modeling of the Variscan
1135 foreland thrust and fold belt crust in NW Spain from ESCIN-1 deep seismic reflection data,
1136 *Tectonophysics*, 269(1–2), 21–32, doi:10.1016/S0040-1951(96)00166-7, 1997.
- 1137 Gallastegui, J., Pulgar, J. A. and Gallart, J.: Alpine tectonic wedging and crustal delamination in
1138 the Cantabrian Mountains (NW Spain), *Solid Earth*, 7(4), 1043–1057, doi:10.5194/se-7-1043-
1139 2016, 2016.
- 1140 García Casquero, J. L., Boelrijk, N. A. I. M., Chacón, J. and Priem, H. N. A.: Rb-Sr evidence for the
1141 presence of Ordovician gsrnites in the deformed basement of the Badajoz-Córdoba belt, SW
1142 Spain, *Geol. Rundschau*, 74(2), 379–384, doi:10.1007/BF01824904, 1985.
- 1143 Gardien, V., Arnaud, N. and Desmurs, L.: Petrology and ar-ar dating of granulites from the
1144 galicia bank (spain): African craton relics in western europe, *Geodin. Acta*, 13(2–3), 103–117,
1145 doi:10.1080/09853111.2000.11105367, 2000.
- 1146 Gómez-Pugnaire, M. T., Azor, A., Fernández-Soler, J. M. and López Sánchez-Vizcaíno, V.: The
1147 amphibolites from the Ossa-Morena/Central Iberian Variscan suture (Southwestern Iberian
1148 Massif): Geochemistry and tectonic interpretation, *Lithos*, 68(1–2), 23–42, doi:10.1016/S0024-
1149 4937(03)00018-5, 2003.
- 1150 Gómez Barreiro, J., Martínez Catalán, J. R., Arenas, R., Castiñeiras, P., Abati, J., Díaz García, F.
1151 and Wijbrans, J. R.: Tectonic evolution of the upper allochthon of the Órdenes complex (
1152 northwestern Iberian Massif): Structural constraints to a polyorogenic peri-Gondwanan
1153 terrane, *Geol. Soc. Am. Spec. Pap.*, 423, 315–332, doi:10.1130/2007.2423(15)., 2007.
- 1154 Hernández Enrile, J. L.: Extensional tectonics of the toledo ductile-brittle shear zone, central
1155 Iberian Massif, *Tectonophysics*, 191(3–4), 311–324, doi:10.1016/0040-1951(91)90064-Y, 1991.
- 1156 Hobbs, B. E., Ord, A., Regenauer-Lieb, K. and Drummond, B.: Fluid reservoirs in the crust and
1157 mechanical coupling between the upper and lower crust, *Earth, Planets Sp.*, 56(12), 1151–
1158 1161, doi:10.1186/BF03353334, 2004.
- 1159 Julivert, M., Fontboté, M., Ribeiro, A. and Conde, L. E.: Mapa tectónico de la Península Ibérica
1160 y Baleares Notas Incluye mapa : Unidades estructurales de la Península Ibérica . Escala 1 :
1161 1.000.000., Instituto Geológico y Minero de España., 1972.
- 1162 Klempere, S. L., Hauge, T. A., Hauser, E. C., Oliver, J. E. and Potter, C. J.: The Moho in the
1163 northern Basin and Range Province, Nevada, along the COCORP 40oN seismic- reflection
1164 transect. (USA), *Geol. Soc. Am. Bull.*, 97(5), 603–618, doi:10.1130/0016-
1165 7606(1986)97<603:TMITNB>2.0.CO;2, 1986.
- 1166 Kossmat, F.: Gliederung des varistischen Gebirgsbaues. Abhandlungen des Sächsischen, in
1167 Abhandlungen des Sächsischen Geologuschen Landesamts, edited by A. des S. G. Landesamts,
1168 p. 39, Leipzig, Heft 1., 1927.
- 1169 Levander, A. R. and Holliger, K.: Small-scale heterogeneity and large-scale velocity structure of
1170 the continental crust, *J. Geophys. Res.*, 97(B6), 8797–8804, doi:10.1029/92JB00659, 1992.
- 1171 Linnemann, U., Pereira, M. F., Jeffries, T. E., Drost, K. and Gerdes, A.: The Cadomian Orogeny



- 1172 and the opening of the Rheic Ocean: The diachrony of geotectonic processes constrained by LA-
1173 ICP-MS U-Pb zircon dating (Ossa-Morena and Saxo-Thuringian Zones, Iberian and Bohemian
1174 Massifs), *Tectonophysics*, 461(1–4), 21–43, doi:10.1016/j.tecto.2008.05.002, 2008.
- 1175 Litak, R. K. and Brown, L. D.: A modern perspective on the Conrad Discontinuity, *Eos, Trans.*
1176 *Am. Geophys. Union*, 70(29), 713–725, doi:10.1029/89EO00223, 1989.
- 1177 López Sánchez-Vizcaíno, V., Gómez-Pugnaire, M. T., Azor, A. and Fernández-Soler, J. M.: Phase
1178 diagram sections applied to amphibolites: A case study from the Ossa-Morena/Central Iberian
1179 Variscan suture (Southwestern Iberian Massif), *Lithos*, 68(1–2), 1–21, doi:10.1016/S0024-
1180 4937(03)00017-3, 2003.
- 1181 Lotze, F.: *Stratigraphie und Tektonik des Keltiberischen Grundgebirges (Spanien),*
1182 *Abhandlungen Gesellschaft der Wissenschaften zu Göttingen, Math. (Abh. Ges. Wiss.*
1183 *Göttingen, Math.-Phys.)*, 14(2), 143–162, 1929.
- 1184 Maggini, M. and Caputo, R.: Sensitivity analysis for crustal rheological profiles: Examples from
1185 the Aegean region, *Ann. Geophys.*, 63(3), 1–29, doi:10.4401/ag-8244, 2020.
- 1186 Martínez Catalán, J. R.: *Estratigrafía y estructura del domo de Lugo (Sector Oeste de la Zona*
1187 *Asturorccidental-Leonesa, Corpus Geologicum Gallaeciae.*, 1985.
- 1188 Martínez Catalán, J. R.: Are the oroclines of the Variscan belt related to late Variscan strike-slip
1189 tectonics?, *Terra Nov.*, 23(4), 241–247, doi:10.1111/j.1365-3121.2011.01005.x, 2011a.
- 1190 Martínez Catalán, J. R.: The Central Iberian arc, an orocline centered in the Iberian Massif and
1191 some implications for the Variscan belt, *Int. J. Earth Sci.*, 101(5), 1299–1314,
1192 doi:10.1007/s00531-011-0715-6, 2011b.
- 1193 Martínez Catalán, J. R., Ayarza, P., Pulgar, J. A., Pérez-Estaún, A., Gallart, J., Marcos, A., Bastida,
1194 F., Álvarez-Marrón, J., González Lodeiro, F., Aller, J., Dañobeitia, J. J., Banda, E., Córdoba, D.
1195 and Comas, M. C.: Results from the ESCIN-N3.3 marine deep seismic profile along the
1196 Cantabrian continental margin, *Rev. Soc. Geol. España*, 8(4), 341–354., 1995.
- 1197 Martínez Catalán, J. R., Arenas, R., Díaz García, F. and Abati, J.: Variscan accretionary complex
1198 of northwest Iberia: Terrane correlation succession of tectonothermal events, *Geology*, 25(12),
1199 1103–1106, doi:10.1130/0091-7613(1997)025<1103:VACONI>2.3.CO;2, 1997.
- 1200 Martínez Catalán, J. R., Fernández-Suárez, J., Jenner, G. A., Belousova, E. and Díez Montes, A.:
1201 Provenance constraints from detrital zircon U–Pb ages in the NW Iberian Massif: implications
1202 for Palaeozoic plate configuration and Variscan evolution, *J. Geol. Soc. London.*, 161(3), 463–
1203 476, doi:10.1144/0016-764903-054, 2004.
- 1204 Martínez Catalán, J. R., Arenas, R., Diágarcía, F., González Cuadra, P., Gómez-Barreiro, J., Abati,
1205 J., Castiñeiras, P., Fernández-Suárez, J., Sánchez Martínez, S., Andonaegui, P., González Clavijo,
1206 E., Díez Montes, A., Rubio Pascual, F. J. and Valle Aguado, B.: Space and time in the tectonic
1207 evolution of the northwestern Iberian Massif: Implications for the Variscan belt, *Mem. Geol.*
1208 *Soc. Am.*, 200(21), 403–423, doi:10.1130/2007.1200(21), 2007.
- 1209 Martínez Catalán, J. R., Álvarez Lobato, F., Pinto, V., Gómez Barreiro, J., Ayarza, P., Villalaín, J. J.
1210 and Casas, A.: Gravity and magnetic anomalies in the allochthonous rdenes Complex (Variscan
1211 belt, northwest Spain): Assessing its internal structure and thickness, *Tectonics*, 31(5), 1–18,
1212 doi:10.1029/2011TC003093, 2012.
- 1213 Martínez Catalán, J. R., Rubio Pascual, F. J., Díez Montes, A., Díez Fernández, R., Gómez



- 1214 Barreiro, J., Dias da Silva, Í., González Clavijo, E., Ayarza, P. and Alcock, J. E.: The late Variscan
1215 HT/LP metamorphic event in NW and Central Iberia: relationships to crustal thickening,
1216 extension, orocline development and crustal evolution, *Geol. Soc. London, Spec. Publ.*, 405(1),
1217 225–247, doi:10.1144/SP405.1, 2014.
- 1218 Martínez Catalán, J. R., Díez Balda, M. A., Escuder Viruete, J., Villar Alonso, P., Ayarza, P.,
1219 Gonzalez Clavijo, E. and Díez Montes, A.: Cizallamientos dúctiles de escala regional en la
1220 provincia de Salamanca, in *Geo-Guias: Rutas Geológicas por la Península Ibérica, Canarias,*
1221 *Sicilia y Marruecos*, edited by M. Diaz Azpiroz, I. Exposito Ramos, S. Llana Fúnez, and B. Bauluz
1222 Lázaro, pp. 109–118, Sociedad Geológica de España., 2019.
- 1223 Martínez García, A.: Seismic characterization and geodynamic significance of the mid-crustal
1224 discontinuity across the Variscan Iberia, *Universidad de Barcelona.*, 2019.
- 1225 Martínez García, E.: El Paleozoico de la Zona Cantábrica Oriental (Noroeste de España), *Trab.*
1226 *Geol.*, 11, 95–127, 1981.
- 1227 Martínez Poyatos, D., Carbonell, R., Palomeras, I., Simancas, J. F., Ayarza, P., Martí, D., Azor, A.,
1228 Jabaloy, A., González Cuadra, P., Tejero, R., Martín Parra, L. M., Matas, J., González Lodeiro, F.,
1229 Pérez-Estaún, A., García Lobón, J. L. and Mansilla, L.: Imaging the crustal structure of the
1230 Central Iberian Zone (Variscan Belt): The ALCUDIA deep seismic reflection transect, *Tectonics*,
1231 31(3), 1–21, doi:10.1029/2011TC002995, 2012.
- 1232 Martínez Poyatos, D. J.: Estructura del borde meridional de la Zona Centroibérica y su relación
1233 con el contacto entre las Zonas Centroibérica y de Ossa-Morena, in *Serie Nova Terra*, 18,
1234 edited by L. X. de Laxe, p. 295, Instituto Universitario de Xeoloxía, A Coruña, Spain., 2002.
- 1235 Matte, P.: The Variscan collage and orogeny (480–290 Ma) and the tectonic definition of the
1236 Armorica microplate: a review - Matte - 2003 - *Terra Nova* - Wiley Online Library, *Terra Nov.*,
1237 13(1997), 122–128 [online] Available from: <http://onlinelibrary.wiley.com/doi/10.1046/j.1365-3121.2001.00327.x/full%5Cnpapers2://publication/uuid/85445613-EAD8-49D7-AE4E-704E3D282C36>, 2001.
- 1240 Matte, P. and Ribeiro, A.: Forme et orientation de l'ellipsoïde de déformation dans la virgation
1241 hercynienne de Galice. Relations avec le plissement et hypothèses sur la genèse de l'arc ibéro-
1242 armoricain, *Comptes Rendus l'Académie des Sci.*, 280, 2825–2828, 1975.
- 1243 Meissner, R.: Rupture, creep, lamellae and crocodiles: happenings in the continental crust,
1244 *Terra Nov.*, 1(1), 17–28, doi:10.1111/j.1365-3121.1989.tb00321.x, 1989.
- 1245 Meissner, R., Rabbal, W. and Kern, H.: Seismic lamination and anisotropy of the lower
1246 continental crust, *Tectonophysics*, 416(1–2), 81–99, doi:10.1016/j.tecto.2005.11.013, 2006.
- 1247 Melekhova, E., Schlaphorst, D., Blundy, J., Kendall, J. M., Connolly, C., McCarthy, A. and
1248 Arculus, R.: Lateral variation in crustal structure along the Lesser Antilles arc from petrology of
1249 crustal xenoliths and seismic receiver functions, *Earth Planet. Sci. Lett.*, 516, 12–24,
1250 doi:10.1016/j.epsl.2019.03.030, 2019.
- 1251 Montero, P., Bea, F., González-Lodeiro, F., Talavera, C. and Whitehouse, M. J.: Zircon ages of
1252 the metavolcanic rocks and metagranites of the Ollo de Sapo Domain in central Spain:
1253 Implications for the Neoproterozoic to Early Palaeozoic evolution of Iberia, *Geol. Mag.*, 144(6),
1254 963–976, doi:10.1017/S0016756807003858, 2007.
- 1255 Ochsner, A.: U-Pb geochronology of the Upper Proterozoic-Lower Paleozoic geodynamic
1256 evolution in the Ossa-Morena Zone (SW Iberia): constraints on the timing of the Cadomian



- 1257 orogeny, University of Zurich, Diss. ETH10, 192., 1993.
- 1258 Okaya, D., Rabbel, W., Beilecke, T. and Hasenclever, J.: P wave material anisotropy of a
1259 tectono-metamorphic terrane: An active source seismic experiment at the KTB super-deep drill
1260 hole, southeast Germany, *Geophys. Res. Lett.*, 31(24), 1–4, doi:10.1029/2004GL020855, 2004.
- 1261 Oliveira, J. T.: Part VI: South Portuguese Zone, stratigraphy and synsedimentary tectonism, in
1262 Pre-Mesozoic Geology of Iberia, edited by E. Dallmeyer, R. D., and Martínez García, pp. 334–
1263 347, Springer, Berlin, Germany., 1990.
- 1264 Oncken, O.: Orogenic mass transfer and reflection seismic patterns - Evidence from DEKORP
1265 sections across the European variscides (central Germany), *Tectonophysics*, 286(1–4), 47–61,
1266 doi:10.1016/S0040-1951(97)00254-0, 1998.
- 1267 Palomeras, I., Carbonell, R., Flecha, I., Simancas, J. F., Ayarza, P., Matas, J., Poyatos, D. M.,
1268 Azor, A., Lodeiro, F. G. and Pérez-Estaún, A.: Nature of the lithosphere across the Variscan
1269 orogen of SW Iberia: Dense wide-angle seismic reflection data, *J. Geophys. Res. Solid Earth*,
1270 114(2), 1–29, 2009.
- 1271 Palomeras, I., Carbonell, R., Ayarza, P., Martí, D., Brown, D. and Simancas, J. F.: Shear wave
1272 modeling and Poisson’s ratio in the Variscan Belt of SW Iberia, *Geochemistry, Geophys.*
1273 *Geosystems*, 12(7), 1–23, doi:10.1029/2011GC003577, 2011.
- 1274 Palomeras, I., Villaseñor, A., Thurner, S., Levander, A., Gallart, J. and Harnafi, M.: Lithospheric
1275 structure of Iberia and Morocco using finite-frequency Rayleigh wave tomography from
1276 earthquakes and seismic ambient noise, *Geochemistry, Geophys. Geosystems*, 1–17,
1277 doi:10.1002/2016GC006657, 2017.
- 1278 Pedreira, D., Pulgar, J. A., Gallart, J. and Díaz, J.: Seismic evidence of Alpine crustal thickening
1279 and wedging from the western Pyrenees to the Cantabrian Mountains (north Iberia), *J.*
1280 *Geophys. Res.*, 108(B4), 1–21, doi:10.1029/2001JB001667, 2003.
- 1281 Pereira, M. F., Chichorro, M., Williams, I. S., Silva, J. B., Fernández, C., Diaz-Azpiroz, M., Apraiz,
1282 A. and Castro, A.: Variscan intra-orogenic extensional tectonics in the Ossa – Morena-Évora –
1283 Aracena – Lora del Río metamorphic belt , SW Iberian Zone (E Massif): SHRIMP zircon U – Th –
1284 Pb geochronology, in *Ancient Orogens and Modern Analogues*, edited by J. B. Murphy, J. D.
1285 Keppie, and A. J. Hynes, pp. 327, 215–237, Geological Society of London, Special Publications.,
1286 2009.
- 1287 Pereira, M. F., Ribeiro, C., Vilallonga, F., Chichorro, M., Drost, K., Silva, J. B., Albardeiro, L.,
1288 Hofmann, M. and Linnemann, U.: Variability over time in the sources of South Portuguese Zone
1289 turbidites: Evidence of denudation of different crustal blocks during the assembly of Pangaea,
1290 *Int. J. Earth Sci.*, 103(5), 1453–1470, doi:10.1007/s00531-013-0902-8, 2014.
- 1291 Pérez-Cáceres, I., Martínez Poyatos, D., Simancas, J. F. and Azor, A.: The elusive nature of the
1292 Rheic Ocean suture in SW Iberia, *Tectonics*, 34(12), 2429–2450, doi:10.1002/2015TC003947,
1293 2015.
- 1294 Pérez-Cáceres, I., Simancas, J. F., Martínez Poyatos, D., Azor, A. and González Lodeiro, F.:
1295 Oblique collision and deformation partitioning in the SW Iberian Variscides, *Solid Earth*, 7(3),
1296 857–872, doi:10.5194/se-7-857-2016, 2016.
- 1297 Pérez-Estaún, A., Bastida, F., Alonso, J. L., Marquínez, J., Aller, J., Alvarez-Marrón, J., Marcos, A.
1298 and Pulgar, J. A.: A thin-skinned tectonics model for an arcuate fold and thrust belt: The
1299 Cantabrian Zone (Variscan Ibero-Armorican Arc), *Tectonics*, 7(3), 517–537,



- 1300 doi:<https://doi.org/10.1029/TC007i003p00517>, 1988.
- 1301 Pérez-Estaún, A., Martínez Catalán, J. R. and Bastida, F.: Crustal thickening and deformation
1302 sequence in the footwall to the suture of the Variscan belt of northwest Spain, *Tectonophysics*,
1303 191(3–4), 243–253, doi:10.1016/0040-1951(91)90060-6, 1991.
- 1304 Pérez-Estaún, A., Pulgar, J. A., Banda, E. and Alvarez-Marrón, J.: Crustal structure of the
1305 external variscides in northwest Spain from deep seismic reflection profiling, *Tectonophysics*,
1306 232(1–4), doi:10.1016/0040-1951(94)90078-7, 1994.
- 1307 Pin, C., Fonseca, P. E., Paquette, J. L., Castro, P. and Matte, P.: The ca. 350 Ma Beja Igneous
1308 Complex: A record of transcurrent slab break-off in the Southern Iberia Variscan Belt?,
1309 *Tectonophysics*, 461(1–4), 356–377, doi:10.1016/j.tecto.2008.06.001, 2008.
- 1310 Pulgar, J. A., Gallart, J., Fernández-Viejo, G., Pérez-Estaún, A. and Álvarez-Marrón, J.: Seismic
1311 image of the Cantabrian Mountains in the western extension of the Pyrenees from integrated
1312 ESCIN reflection and refraction data, *Tectonophysics*, 264(1–4), 1–19, doi:10.1016/S0040-
1313 1951(96)00114-X, 1996.
- 1314 Quesada, C. and Dallmeyer, R. D.: Tectonothermal evolution of the Badajoz-Córdoba shear
1315 zone (SW Iberia): characteristics and ⁴⁰Ar/³⁹Ar mineral age constraints, *Tectonophysics*,
1316 231(1–3), 195–213, doi:10.1016/0040-1951(94)90130-9, 1994.
- 1317 Quintana, L., Pulgar, J. A. and Alonso, J. L.: Displacement transfer from borders to interior of a
1318 plate: A crustal transect of Iberia, *Tectonophysics*, 663, 378–398,
1319 doi:10.1016/j.tecto.2015.08.046, 2015.
- 1320 Rat, P.: The Basque-Cantabrian basin between the Iberian and European plates: Some facts but
1321 still many problems, *Rev. la Soc. geológica España*, 1(3–4), 327–348, 1988.
- 1322 Ries, A. C. and Shackleton, R. M.: Catazonal Complexes of North-West Spain and North
1323 Portugal, Remnants of a Hercynian Thrust Plate, *Nat. Phys. Sci.*, 234(47), 65–68,
1324 doi:10.1038/physci234065a0, 1971.
- 1325 Robardet, M.: Alternative approach to the Variscan Belt in southwestern Europe: Preorogenic
1326 paleobiogeographical constraints, *Spec. Pap. Geol. Soc. Am.*, 364, 1–15, doi:10.1130/0-8137-
1327 2364-7.1, 2002.
- 1328 Robardet, M. and Gutiérrez Marco, J. C.: Ossa-Morena Zone. Stratigraphy. Passive Margin
1329 Phase (Ordovician-Silurian-Devonian), in *Pre-Mesozoic Geology of Iberia*, edited by R. D.
1330 Dallmeyer and E. Martínez García, pp. 267–272, Springer-Verlag, Berlin., 1990.
- 1331 Rodrigues, B., Chew, D. M., Jorge, R. C. G. S., Fernandes, P., Veiga-Pires, C. and Oliveira, J. T.:
1332 Detrital zircon geochronology of the Carboniferous Baixo Alentejo Flysch Group (South
1333 Portugal); Constraints on the provenance and geodynamic evolution of the South Portuguese
1334 Zone, *J. Geol. Soc. London.*, 172, 294–308, doi:10.1144/jgs2013-084, 2015.
- 1335 Ross, A. R., Brown, L. D., Pananont, P., Nelson, K. D., Klemperer, S. L., Haines, S., Wenjin, Z. and
1336 Jingru, G.: Deep reflection surveying in central Tibet: Lower-crustal layering and crustal flow,
1337 *Geophys. J. Int.*, 156(1), 115–128, doi:10.1111/j.1365-246X.2004.02119.x, 2004.
- 1338 Royden, L.: Coupling and decoupling of crust and mantle in convergent orogens: Implications
1339 for strain partitioning in the crust, *J. Geophys. Res.*, 101(B8), 17679–17705, 1996.
- 1340 Rubio Pascual, F. J., Arenas, R., Martínez Catalán, J. R., Rodríguez Fernández, L. R. and



- 1341 Wijbrans, J. R.: Thickening and exhumation of the Variscan roots in the Iberian Central System:
1342 Tectonothermal processes and $40\text{Ar}/39\text{Ar}$ ages, *Tectonophysics*, 587, 207–221,
1343 doi:10.1016/j.tecto.2012.10.005, 2013.
- 1344 Sánchez-García, T., Quesada, C., Bellido, F., Dunning, G. R. and González del Tánago, J.: Two-
1345 step magma flooding of the upper crust during rifting: The Early Paleozoic of the Ossa Morena
1346 Zone (SW Iberia), *Tectonophysics*, 461(1–4), 72–90, doi:10.1016/j.tecto.2008.03.006, 2008.
- 1347 Sánchez-García, T., Bellido, F., Pereira, M. F., Chichorro, M., Quesada, C., Pin, C. and Silva, J. B.:
1348 Rift-related volcanism predating the birth of the Rheic Ocean (Ossa-Morena zone, SW Iberia),
1349 *Gondwana Res.*, 17(2–3), 392–407, doi:10.1016/j.gr.2009.10.005, 2010.
- 1350 Sánchez de Posada, L. C., Martínez Chacón, M. L., Méndez Fernández, C., Menéndez Alvarez,
1351 J.R. Truyols, J. and Villa, E.: Carboniferous Pre-Stephanian rocks of the Asturian-Leonese
1352 Domain (Cantabrian Zone), in *Pre-Mesozoic Geology of Iberia*, edited by R. D. Dallmeyer and E.
1353 Martínez García, pp. 24–33, Springer-Verlag., 1990.
- 1354 Sánchez Martínez, S., Arenas, R., Andonaegui, P., Martínez Catalán, J. R. and Pearce, J. A.:
1355 Geochemistry of two associated ophiolites from the Cabo Ortegal Complex (Variscan belt of
1356 NW Spain), *Mem. Geol. Soc. Am.*, 200(23), 445–467, doi:10.1130/2007.1200(23), 2007.
- 1357 Schmelzbach, C., Juhlin, C., Carbonell, R. and Simancas, J. F.: Prestack and poststack migration
1358 of crooked-line seismic reflection data: A case study from the South Portuguese Zone fold belt,
1359 southwestern Iberia, *Geophysics*, 72(2), 9–18, doi:10.1190/1.2407267, 2007.
- 1360 Schmelzbach, C., Simancas, J. F., Juhlin, C. and Carbonell, R.: Seismic reflection imaging over
1361 the South Portuguese Zone fold-and-thrust belt, SW Iberia, *J. Geophys. Res. Solid Earth*, 113(8),
1362 1–16, doi:10.1029/2007JB005341, 2008.
- 1363 Seyferth, M. and Henk, A.: Syn-convergent exhumation and lateral extrusion in continental
1364 collision zones - Insights from three-dimensional numerical models, *Tectonophysics*, 382(1–2),
1365 1–29, doi:10.1016/j.tecto.2003.12.004, 2004.
- 1366 Shelley, D. and Bossière, G.: A new model for the Hercynian Orogen of Gondwanan France and
1367 Iberia, *J. Struct. Geol.*, 22(6), 757–776, doi:10.1016/S0191-8141(00)00007-9, 2000.
- 1368 Simancas, J. F., Martínez Poyatos, D., Expósito, I., Azor, A. and González Lodeiro, F.: The
1369 structure of a major suture zone in the SW Iberian massif: The Ossa-Morena/central Iberian
1370 contact, *Tectonophysics*, 332(1–2), 295–308, doi:10.1016/S0040-1951(00)00262-6, 2001.
- 1371 Simancas, J. F., Carbonell, R., González Lodeiro, F., Pérez Estaún, A., Juhlin, C., Ayarza, P.,
1372 Kashubin, A., Azor, A., Martínez Poyatos, D., Almodóvar, G. R., Pascual, E., Sáez, R. and
1373 Expósito, I.: Crustal structure of the transpressional Variscan orogen of SW Iberia: SW Iberia
1374 deep seismic reflection profile (IBERSEIS), *Tectonics*, 22(6), doi:10.1029/2002TC001479, 2003.
- 1375 Simancas, J. F., Carbonell, R., Gonzalez Lodeiro, F., Pérez-Estaún, A., Juhlin, C., Ayarza, P.,
1376 Kashubin, A., Azor, A., Martínez Poyatos, D., Saez, R., Almodovar, G. R., Pascual, E., Flecha, I.
1377 and Marti, D.: Transpressional collision tectonics and mantle plume dynamics: the Variscides of
1378 southwestern Iberia, *Geol. Soc. London, Mem.*, 32(1), 345–354, 2006.
- 1379 Simancas, J. F., Ayarza, P., Azor, A., Carbonell, R., Martínez Poyatos, D., Pérez-Estaún, A. and
1380 González Lodeiro, F.: A seismic geotraverse across the Iberian Variscides: Orogenic shortening,
1381 collisional magmatism, and orocline development, *Tectonics*, 32(3), 417–432,
1382 doi:10.1002/tect.20035, 2013.



- 1383 Snelson, C. M., Randy Keller, G., Miller, K. C., Rumpel, H. M. and Prodehl, C.: Regional Crustal
 1384 Structure Derived from the CD-ROM 99 Seismic Refraction/Wide-Angle Reflection Profile: The
 1385 Lower Crust and Upper Mantle, in *The Rocky Mountain Region: An Evolving Lithosphere: Tectonics, Geochemistry, and Geophysics*, pp. 271–291., 2013.
- 1387 Spear, F. S.: *Metamorphic Phase Equilibria and pressure-temperature-time paths*, Monograph,
 1388 edited by M. Mineralogical Society of America, Chelsea., 1993.
- 1389 Stille, H.: *Grundfragen der Vergleichenden. Tectonik*, Gebrueder Borntragen, Berlin., 1924.
- 1390 Taner, M. T. and Sheriff, R. E.: Application of Amplitude, Frequency, and Other Attributes to
 1391 Stratigraphic and Hydrocarbon Determination, in *AAPG Memoir, Seismic Stratigraphy —*
 1392 *Applications to Hydrocarbon Exploration*, vol. 26, pp. 301–327., 1977.
- 1393 Teixell, A., Labaume, P., Ayarza, P., Espurt, N., de Saint Blanquat, M. and Lagabrielle, Y.: Crustal
 1394 structure and evolution of the Pyrenean-Cantabrian belt: A review and new interpretations
 1395 from recent concepts and data, *Tectonophysics*, 724–725(July 2017), 146–170,
 1396 doi:10.1016/j.tecto.2018.01.009, 2018.
- 1397 Truyols, J., Arbizu, M., Garcia-Alcalde, J. L., Garcia-López, S., Mendez-Bendia, I., Soto, F. and
 1398 Truyols, M.: The Asturian-Leonese Domain (Cantabrian Zone), in *Pre-Mesozoic Geology of*
 1399 *Iberia*, edited by R. D. Dallmeyer and E. Martínez García, pp. 10–19, Springer-Verlag., 1990.
- 1400 de Vicente, G., Giner, J. L., Muñoz-Martí, A., González-Casado, J. M. and Lindo, R.:
 1401 Determination of present-day stress tensor and neotectonic interval in the Spanish Central
 1402 System and Madrid Basin, central Spain, *Tectonophysics*, 266(1–4), 405–424,
 1403 doi:10.1016/S0040-1951(96)00200-4, 1996.
- 1404 Villaseca, C., Orejana, D. and Belousova, E. A.: Recycled metagneous crustal sources for S- and
 1405 I-type Variscan granitoids from the Spanish Central System batholith: Constraints from Hf
 1406 isotope zircon composition, *Lithos*, 153, 84–93, doi:10.1016/j.lithos.2012.03.024, 2012.
- 1407 Wever, T.: The Conrad discontinuity and the top of the reflective lower crust-do they
 1408 coincide?, *Tectonophysics*, 157(1–3), 39–58, doi:10.1016/0040-1951(89)90339-9, 1989.
- 1409 Xiaobo, H. and Tae Kyung, H.: Evidence for strong ground motion by waves refracted from the
 1410 Conrad discontinuity, *Bull. Seismol. Soc. Am.*, 100(3), 1370–1374, doi:10.1785/0120090159,
 1411 2010.

1412

1413

1414 Table 1: Acquisition parameters of the NI seismic profiles shown from figures 3 to 8 and
 1415 former processing flows. These are grouped according to their similarities.

1416	Acquisition parameters	ESCIN-1 (onshore)	ESCIN-2 (onshore)
1417	Source	Dynamite-single-hole	Dynamite-single-hole
1418	Charge	20 kg at 24 m depth	20 kg at 24 m depth
1419	Trace Interval	60 m	60 m
1420	# of traces	240	240
1421	Spread configuration	Symmetrical Split-spread	Symmetrical Split-spread
1422	Fold	30	30
1423	Geophones per group	18	18



1424	Spread length	14.5 km	14.5 km
1425	Sample interval		4 ms
1426			
1427		ESCIN-3.2 and ESCIN-3.3 (offshore)	
1428			
1429	Source	Airgun (5490 cu.in)	
1430	Shot spacing	75 m	
1431	Receiver interval	12.5 m	
1432	Spread length	4500 m	
1433	Fold	30	
1434	Internal offset	240 m	
1435	Sample rate	4 ms	
1436	Record length	20 s	
1437			
1438			
1439		IBERSEIS (onshore)	ALCUDIA (onshore)
1440			
1441	Source	4, 22T vibrators	4 (+1), 22T vibrators
1442	Recording instrument	SERCEL 388, 10 Hz	SERCEL 388, 10 Hz
1443	# active channels	240 minimum	240 minimum
1444	Station spacing	35 m	35 m
1445	Station configuration	12 geophones	12 geophones
1446	Source spacing	70 m	70 m
1447	Sweep frequencies	non-linear 8-80 Hz	non-linear 8-80 Hz
1448	Sweep length	20 s	20 s
1449	Listening time	40 s	40 s
1450	Sample rate	2 ms	4 ms
1451	Spread type	Asymmetric split-spread	Asymmetric split-spread
1452	Nominal fold	60 (minimum)	60 (minimum)

1453
 1454
 1455
 1456 Figure captions
 1457

1458 Figure 1: Map of the Iberian Peninsula showing the outcrops of the Variscan basement and the
 1459 subdivision in zones of the Iberian Massif. The main strike-slip shear zones and gneiss domes
 1460 are included. Blue lines show the position of normal incidence seismic reflection profiles and
 1461 that of the CIMDEF transect. Abbreviations: Allochthonous complexes of NW Iberia: B:
 1462 Bragança; CO: Cabo Ortegal; M: Morais; MT: Malpica-Tui; O: Órdenes. Strike-slip shear zones:
 1463 BCSZ: Badajoz-Córdoba; DBSZ: Douro-Beira; JPSZ: Juzbado-Penalva; PTSZ: Porto-Tomar; SISZ:
 1464 Southern Iberian. See legend for other abbreviations. Traces of the main Variscan folds and the
 1465 Variscan granitoids are also included.

1466 Figure 2: Processing flow carried over the SEG-Y original stack sections. This task was
 1467 geared to improve and homogenize the resolution of the seismic images while creating
 1468 new migrated sections. See Martínez García, (2019) for further details.

1469 Figure 3: Migrated section of the NI seismic profile ESCIN-1 (Fig. 1), without (a) and with
 1470 interpretation (b). A sketch of the most important features is presented in (c). CDP:



- 1471 Common Depth Point. TWT: Two-way travel time. WALZ: West Asturian-Leonese Zone. CZ:
1472 Cantabrian Zone. The position of the Narcea Antiform is indicated.
- 1473 Figure 4: Migrated section of the NI seismic profile ESCIN-2 (Fig. 1), without (a) and with
1474 interpretation (b). A sketch of the most important features is presented in (c). CDP:
1475 Common Depth Point. TWT: Two-way travel time. WALZ: West Asturian-Leonese Zone. CZ:
1476 Cantabrian Zone. DB: Duero Basin.
- 1477 Figure 5: Migrated section of the NI seismic profile ESCIN-3.3 (Fig. 1), without (a) and with
1478 interpretation (b). A sketch of the most important features is presented in (c). CDP:
1479 Common Depth Point. TWT: Two-way travel time. WALZ: West Asturian-Leonese Zone. CIZ:
1480 Central Iberian Zone. The offshore projection of the Viveiro Fault is indicated.
- 1481 Figure 6: Migrated section of the NI seismic profile ESCIN-3.2 (Fig. 1), without (a) and with
1482 interpretation (b). A sketch of the most important features is presented in (c). CDP:
1483 Common Depth Point. TWT: Two-way travel time. GTMZ: Galicia-Trás-os-Montes Zone.
- 1484 Figure 7: Migrated section of the NI seismic profile ALCUDIA (Fig. 1), without (a) and with
1485 interpretation (b). A sketch of the most important features is presented in (c). CDP:
1486 Common Depth Point. TWT: Two-way travel time. CIZ: Central Iberian Zone. CU: Central
1487 Unit.
- 1488 Figure 8: Migrated section of the NI seismic profile IBERSEIS (Fig. 1), without (a) and with
1489 interpretation (b). A sketch of the most important features is presented in (c). CDP:
1490 Common Depth Point. TWT: Two-way travel time. CIZ: Central Iberian Zone. CU: Central
1491 Unit. OMZ: Ossa-Morena Zone. RORS: Rheic ocean reworked suture. SPZ: South Portuguese
1492 Zone.
- 1493 Figure 9: Joint geological interpretation of all the seismic sections (normal incidence and
1494 seismic noise) whose location is shown in figure 1. (a): ESCIN-1, ESCIN3-3 and ESCIN-3.2.
1495 (b): ALCUDIA and IBERSEIS. (c): CIMDEF. Special attention should be paid to the depth and
1496 geometry of the Moho and mid-crustal discontinuity. Alpine structures (i.e. crustal
1497 thickening) appear in ESCIN-1 and in CIMDEF. The rest are Variscan features.
- 1498 Figure 10: Map of the Moho depth as derived from tomography of shear waves (seismic
1499 noise and earthquakes, Palomeras et al., 2017) with the projection of the seismic profiles
1500 already shown in figure 1 and described along the text. A sketch of the geometry of the
1501 main discontinuities (Moho and Conrad) is also shown.

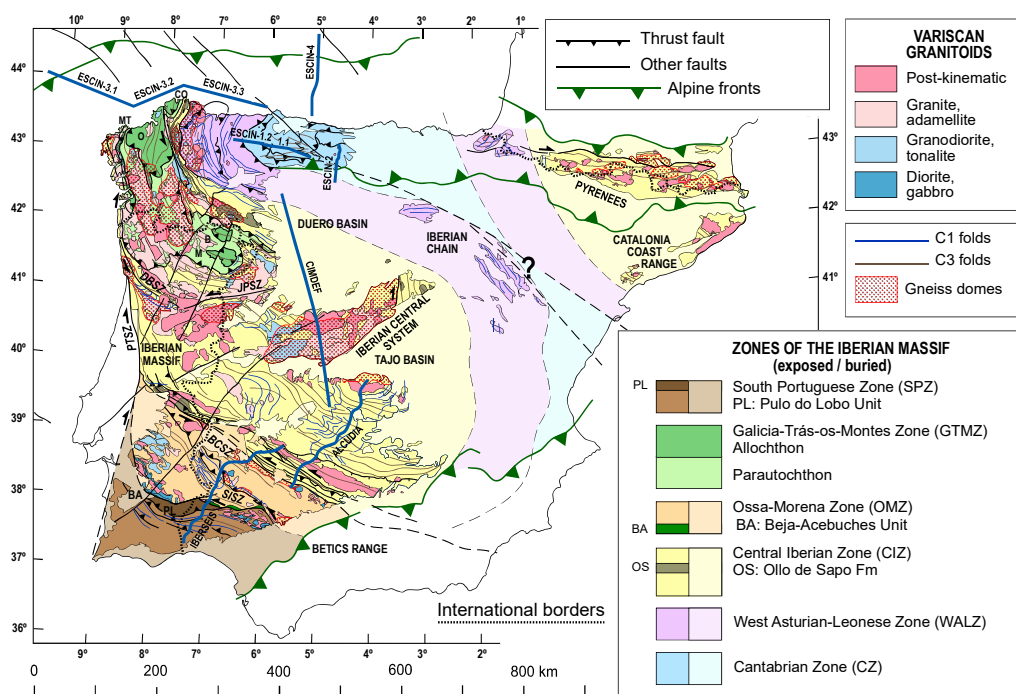


Figure 1

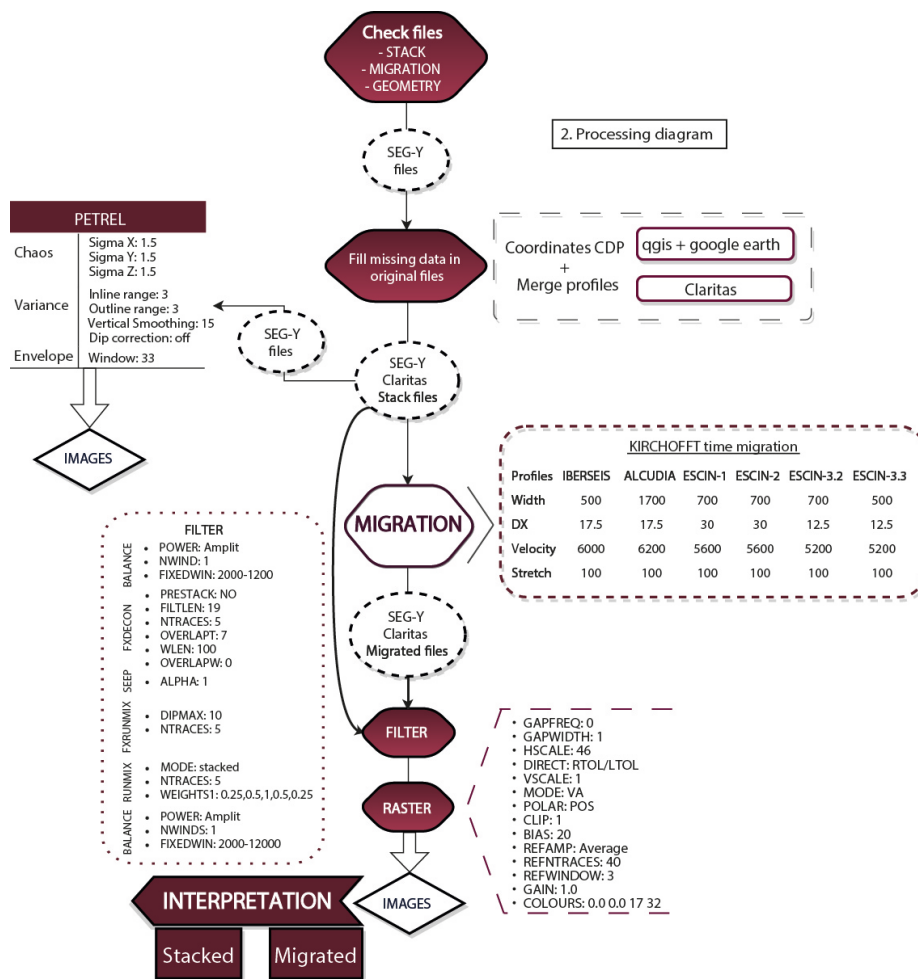


Figure 2

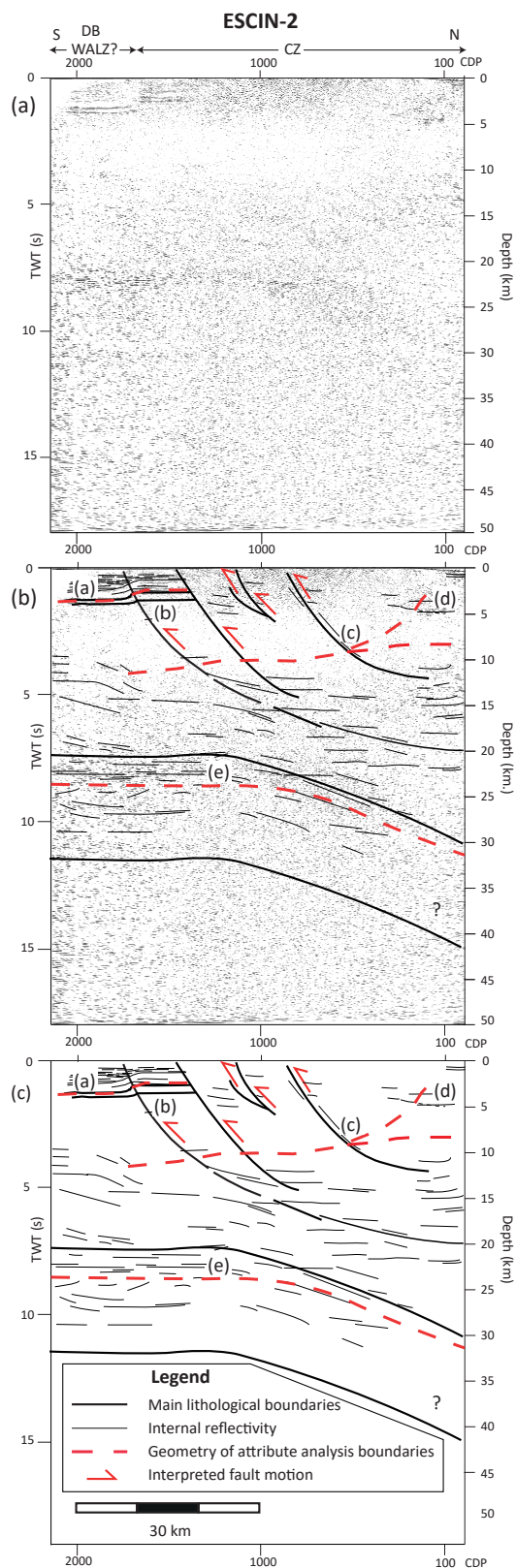


Figure 4

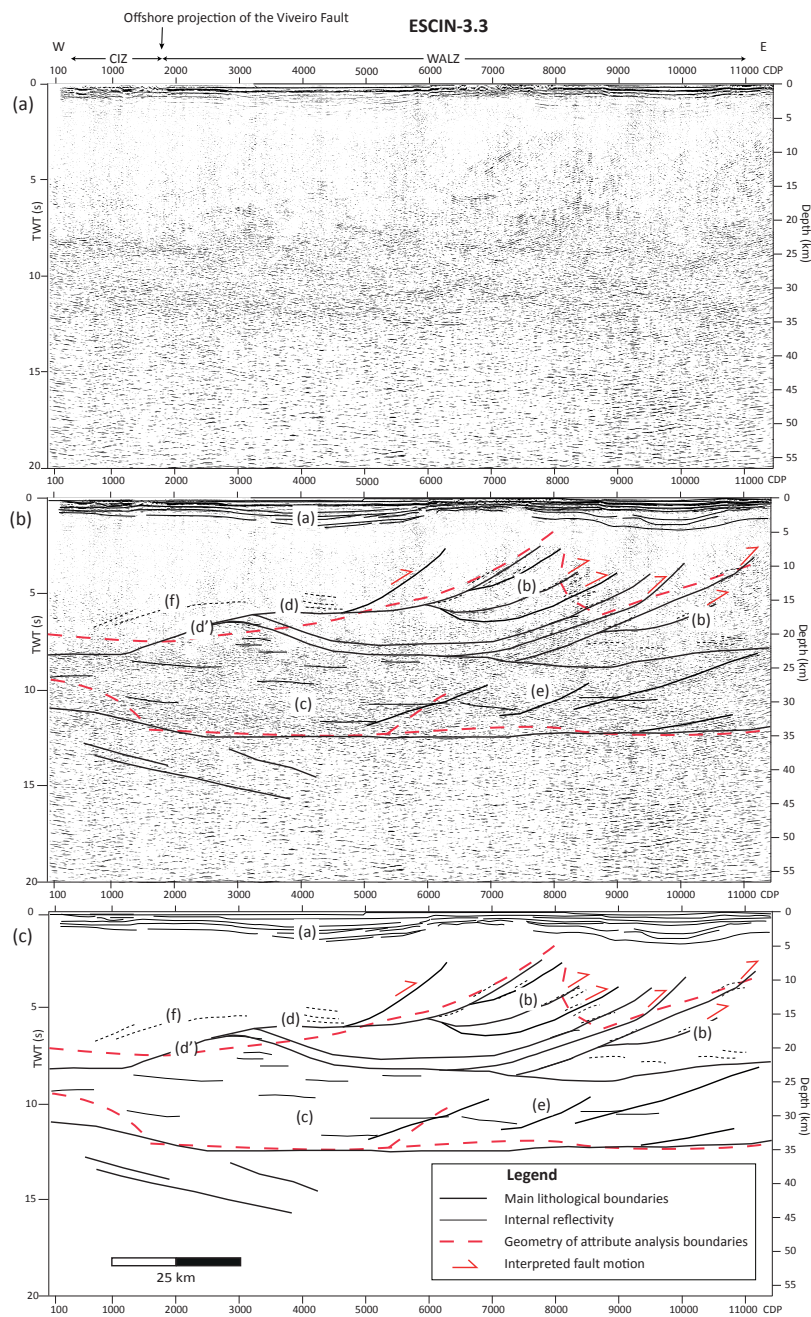


Figure 5

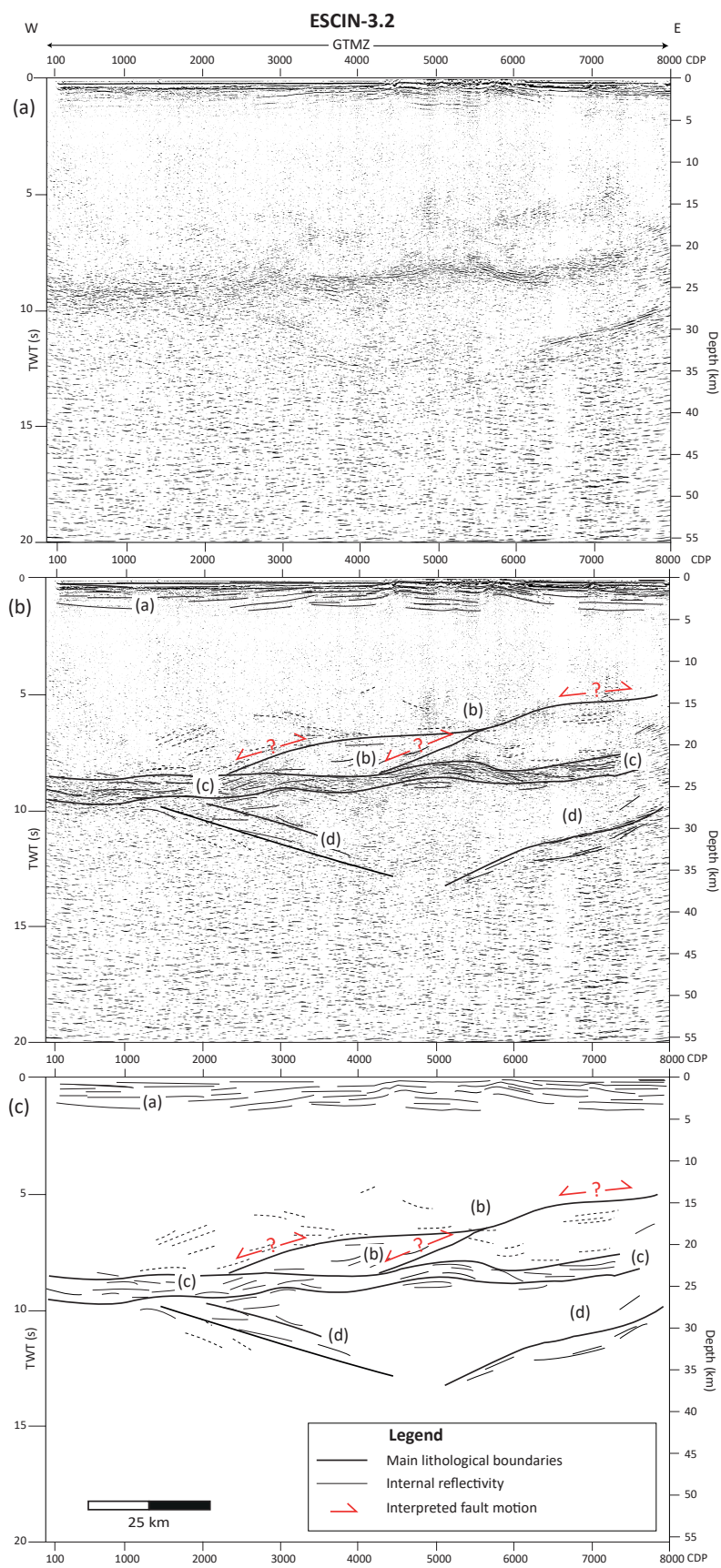


Figure 6

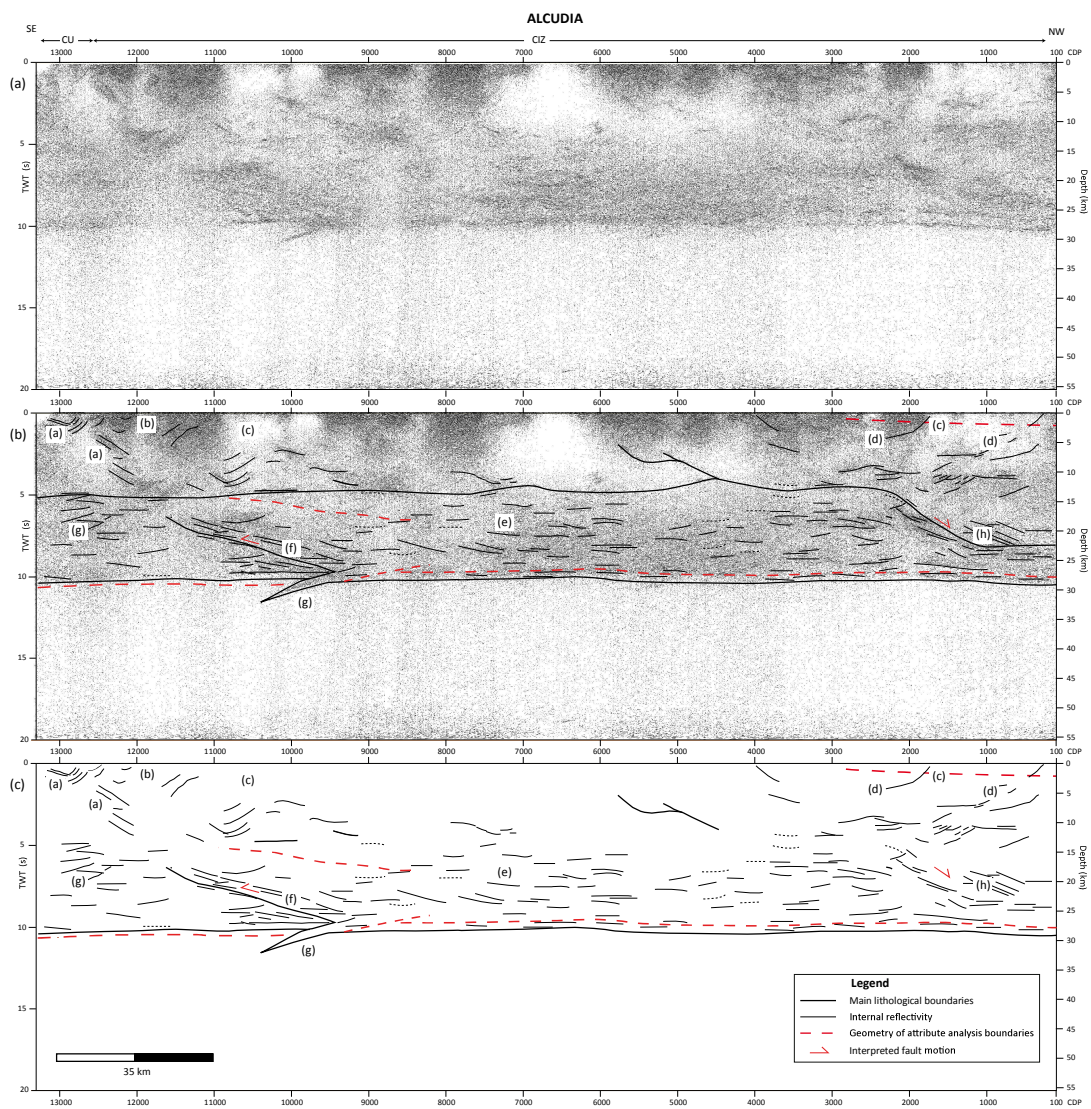


Figure 7

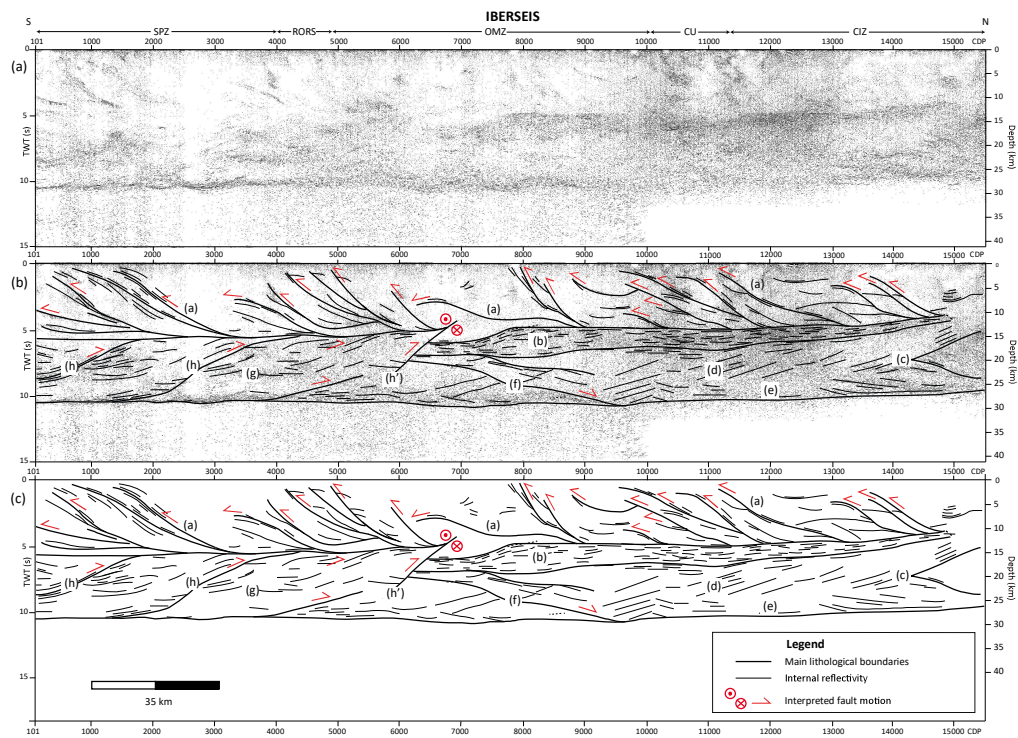


Figure 8

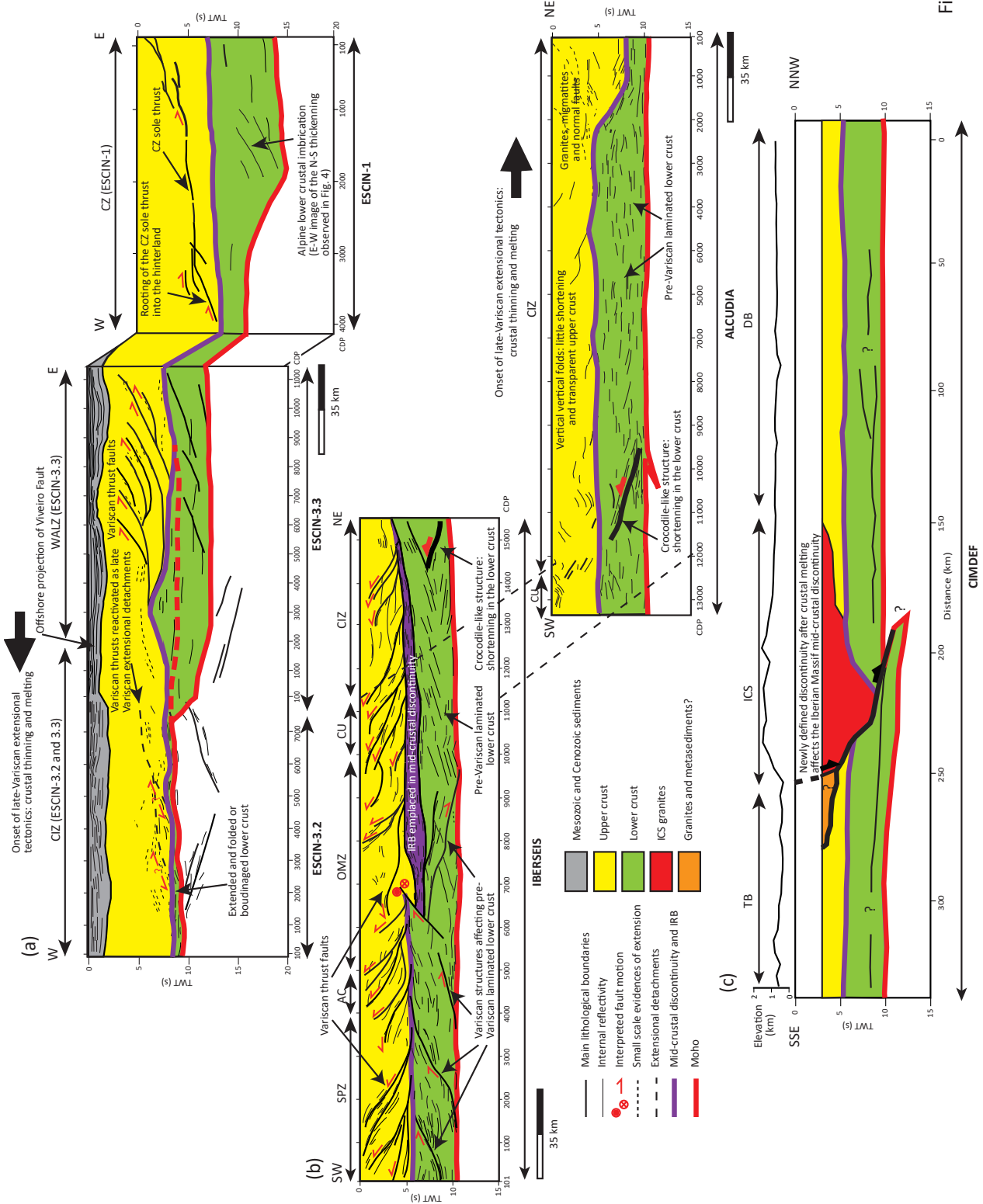


Figure 9

